Pergamon

Continental Shelf Research, Vol. 16, No. 15, pp. 2005–2039, 1996

PII: S0278-4343(96)00032-5
0278-4343/96 $15.00 + 0.00

The long-term salinity field in San Francisco Bay

R. J. UNCLES* and D. H. PETERSON†

(*Received* 1 *June* 1994; *in revised form* 9 *January* 1996; *accepted* 9 *July* 1996)

Abstract—Data are presented on long-term salinity behaviour in San Francisco Bay, California. A two-level, width averaged model of the tidally averaged salinity and circulation has been written in order to interpret the long-term (days to decades) salinity variability. The model has been used to simulate daily averaged salinity in the upper and lower levels of a 51 segment discretization of the Bay over the 22-yr period 1967–1988. Monthly averaged surface salinity from observations and monthly-averaged simulated salinity are in reasonable agreement. Good agreement is obtained from comparison with daily averaged salinity measured in the upper reaches of North Bay.

The salinity variability is driven primarily by freshwater inflow with relatively minor oceanic influence. All stations exhibit a marked seasonal cycle in accordance with the Mediterranean climate, as well as a rich spectrum of variability due to extreme inflow events and extended periods of drought. Monthly averaged salinity intrusion positions have a pronounced seasonal variability and show an approximately linear response to the logarithm of monthly averaged Delta inflow. Although few observed data are available for studies of long-term salinity stratification, modelled stratification is found to be strongly dependent on freshwater inflow; the nature of that dependence varies throughout the Bay. Near the Golden Gate, stratification tends to increase up to very high inflows. In the central reaches of North Bay, modelled stratification maximizes as a function of inflow and further inflow reduces stratification. Near the head of North Bay, lowest summer inflows are associated with the greatest modelled stratification. Observations from the central reaches of North Bay show marked spring–neap variations in stratification and gravitational circulation, both being stronger at neap tides. This spring–neap variation is simulated by the model. A feature of the modelled stratification is a hysteresis in which, for a given spring–neap tidal range and fairly steady inflows, the stratification is higher progressing from neaps to springs than from springs to neaps.

The simulated responses of the Bay to perturbations in coastal sea salinity and Delta inflow have been used to further delineate the time-scales of salinity variability. Simulations have been performed about low inflow, steady-state conditions for both salinity and Delta inflow perturbations. For salinity perturbations a small, sinusoidal salinity signal with a period of 1 yr has been applied at the coastal boundary as well as a pulse of salinity with a duration of one day. For Delta inflow perturbations a small, sinusoidally varying inflow signal with a period of 1 yr has been superimposed on an otherwise constant Delta inflow, as well as a pulse of inflow with a duration of one day. Perturbations in coastal salinity dissipate as they move through the Bay. Seasonal perturbations require about 40–45 days to propagate from the coastal ocean to the Delta and to the head of South Bay. The response times of the model to perturbations in freshwater inflow are faster than this in North Bay and comparable in South Bay. In North Bay, time-scales are

*Plymouth Marine Laboratory, Plymouth, PL1 3DH, U.K.
†U.S. Geological Survey, Menlo Park, CA, U.S.A.

consistent with advection due to lower level, up-estuary transport of coastal salinity perturbations; for inflow perturbations, faster response times arise from both upper level, down-estuary advection and much faster, down-estuary migration of isohalines in response to inflow volume continuity. In South Bay, the dominant time-scales are governed by tidal dispersion.

1. INTRODUCTION

With the exception of the Strait of Juan de Fuca, San Francisco Bay is the most prominent embayment on the western coast of the United States [(Fig. 1(a)]. The Bay consists of two distinct subestuaries. The North Bay lies between the Pacific Ocean at the Golden Gate of San Francisco and the confluence of the Sacramento–San Joaquin Rivers (the Delta) and comprises San Pablo Bay, Carquinez Strait and Suisun Bay. The South Bay lies between the Golden Gate and the Guadalupe and Coyote Creeks near San Jose, at the head of the Bay [Fig. 1(b)]. The North Bay is a strongly tidal, partially mixed estuary, whereas the South Bay is a strongly tidal, lagoon-type estuary in which freshwater inflows are small.

The purpose of this paper is to present data on the long-term behaviour of salinity within the Bay. An intertidal model of the long-term salinity is developed in order to aid interpretation. Simulated data are compared with observed surface salinity data from seven stations over the 22-yr period covering water years 1967–1988. Station positions and their geographical relation to the in-plan segmentation of the model Bay are shown in Fig. 1(b). The model is subsequently used to investigate: (1) the behaviour of the freshwater–saltwater interface (FSI) and its dependence on freshwater inflows; (2) intertidal salinity stratification within the Bay and its dependence on inflows and spring–neap tidal state (*TS*); and (3) the characteristic response time-scales of the Bay to perturbations in both coastal salinity and freshwater inflows.

The interpretative salinity model provides a two-level, width averaged, multi-segment simulation of the subtidal water circulation and salt balance. The use of a two-level model does not imply that the Bay is two-layered, but rather that the model attempts to simulate the level averaged salinity and mixing within each level. Tidal current speeds throughout the Bay are derived from a separately run hydrodynamical model, the results from which are tabulated within the salinity model and used to specify tidal mixing. During 1987–1992 a prolonged drought in the region produced much lower than usual freshwater inflows to the Bay. In consequence, there was heightened concern about the possibility of increased salt intrusion (long-term, up-estuary movement of the FSI) and its effects on the ecology and water "quality" of the region. The model, if applied to the Bay's biogeochemistry and if capable of portraying the variability within multi-year episodes, could provide greater insight into the response of the ecosystem to such drought events.

There has been considerable modelling work undertaken on the Bay (see the review by Smith and Cheng, 1989). Laterally averaged, intratidal, hydrodynamic and salinity modelling studies of North Bay have been presented by Ford *et al.* (1990). They demonstrated, from observations, the dependence of salinity stratification in North Bay on Delta inflow and showed that good agreement between measured and modelled salinity at a station in Suisun Bay [Fig. 1(a)] could be achieved over a low inflow period of a few days. Results of depth averaged, intratidal modelling of the hydrodynamics and salinity of Suisun Bay have been presented by Smith and Cheng (1987). The lack of an observed, initial salinity distribution prevented a quantitative comparison of the computed and measured salinities within the Bay. However, an important conclusion arising from this

study was that net changes in salinity were small over a few tidal cycles, despite large changes during a tidal cycle. A three-dimensional, intratidal model of the hydrodynamics and salinity in San Pablo Bay [Fig. 1(a)] generally provided very good agreement between measured and simulated data (discussed by Smith and Cheng, 1989); the model used a 2 min time step and closely reproduced the observed vertical stratification in salinity of between 2 and 8 during a typical tidal cycle. Rather than attempt simulations of several months in order to achieve "spin-up" in the three-dimensional model, the initial salinity was specified from observations.

Although these studies have made great progress in describing and understanding the tidal and higher frequency variability within the Bay, it is clear that an intertidal model is needed to assist with the dynamical interpretation of long-term salinity variability. Such a model would complement statistical studies and be of value to the prediction of consequences arising from short-period climate variability and possible long-term climate changes (Peterson *et al.*, 1987, 1989; Cayan and Peterson, 1989, 1993). Intertidal equations have previously been derived from the fundamental intratidal equations and have been applied to San Francisco Bay studies (Cheng *et al.*, 1989; Feng *et al.*, 1986a,b). However, in view of the difficulty of implementing these equations on the complex geometry of the Bay and the "weakly nonlinear" assumptions inherent in their validity, we have preferred to adopt a "box model" approach. Because there is reasonable agreement between "box model" simulations and measurements, we consider that the model will provide useful predictions. For the time-scales of interest here, more complex models do not necessarily yield more accurate simulations. This approach is therefore an attractive interim step while we await a full description of the complex, intertidal hydrodynamics and salinity variations within the Bay from long-term simulations (over months and years of simulated time) obtained using future generations of intratidal, three-dimensional, hydrodynamic models.

2. ENVIRONMENTAL CONDITIONS AND OBSERVATIONS

During the late Cenozoic, the Bay comprised part of the drainage basin of the ancestral San Joaquin, Sacramento and Coyote Rivers. Following the last ice age, rising sea level began its most recent incursion into the Bay, about 10,000 years BP. Present environmental conditions within the Bay are dominated by the influences of freshwater inflows from the San Joaquin and Sacramento Rivers Delta [Fig. 1(a)] and the propagation of Pacific tides through the Golden Gate (Conomos *et al.*, 1985).

2.1. *Freshwater inflow*

Considering annual freshwater inflow to the Bay, 90% discharges from the Sacramento–San Joaquin Delta and 10% from streams and precipitation. The inflow comprises precipitation runoff during winter and snowmelt runoff from the Sierra Nevada during spring and early summer (Conomos *et al.*, 1985). The monthly averaged data for Delta inflow, South Bay inflow, estimated evaporation and precipitation over the Bay during water years 1967–1988 (1 October 1966–30 September 1988) are given in Fig. 2(a)–(d). Delta inflow data are from the California Department of Water Resources daily flow estimates. Average inflow for the 22 yrs was 870 $m^3 s^{-1}$. This flow is not adjusted for fluctuations in Delta volume, such as might occur in response to tidal and wind-stress

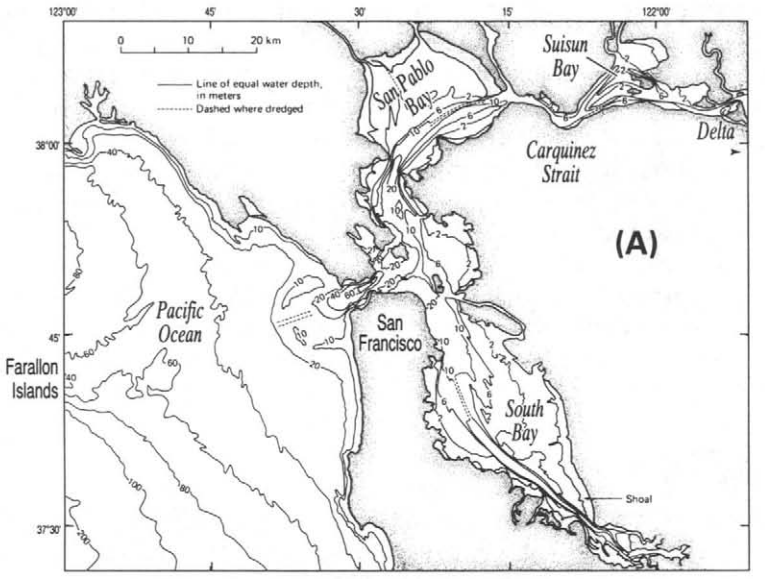
123°00'
45'
30'
15'
122°00'
0 10 20 km
Line of equal water depth, in meters
Dashed where dredged
Suisun Bay
San Pablo Bay
Delta
Carquinez Strait
(A)
38°00'
Pacific Ocean
San Francisco
Farallon Islands
45'
South Bay
Shoal
37°30'

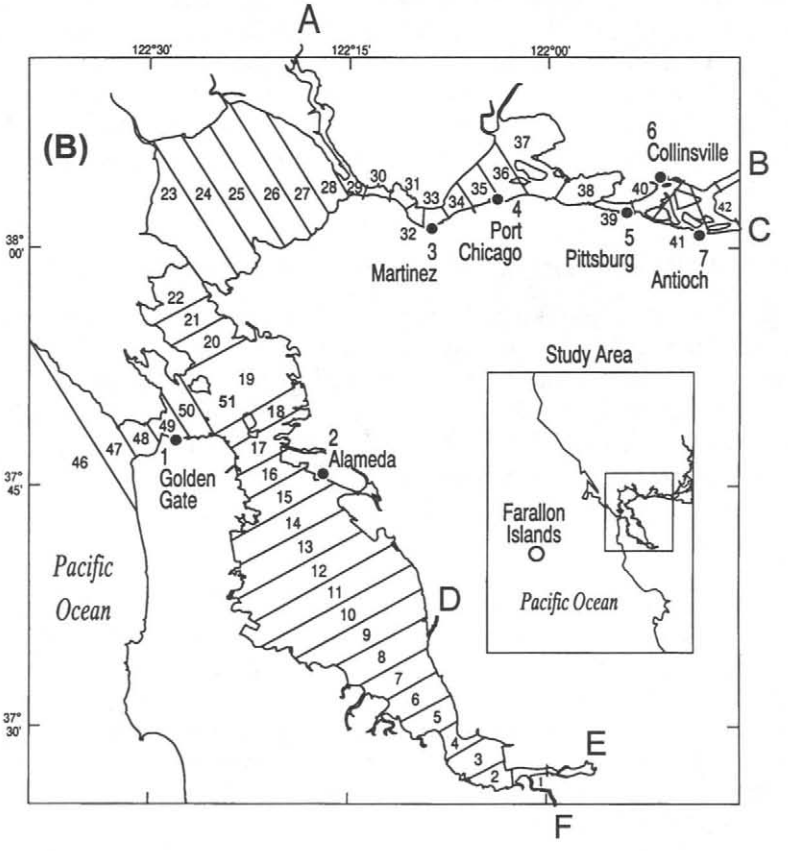
A
122°30'
122°15'
122°00'
(B)
6 Collinsville
B
C
38° 00'
3 Martinez
4 Port Chicago
5 Pittsburg
7 Antioch
Study Area
Farallon Islands
Pacific Ocean
2 Alameda
1 Golden Gate
37° 45'
Pacific Ocean
D
37° 30'
E
F

fluctuations. Errors are thought to be relatively small (<10%) on a monthly time-scale, except for extreme low or, perhaps, high flows.

Maximum, mean daily freshwater Delta inflow of 1.8×10^4 m^3 s^{-1} for water years 1967–1988 occurred during the freshwater flood (spate) of February 1986 (water year 1986). Two very long periods of low inflows occurred. Between August 1975 and October 1977, California experienced a drought for which the mean inflow was only 190 m^3 s^{-1}, compared with the average inflow of 870 m^3 s^{-1}. The second long period of low inflows

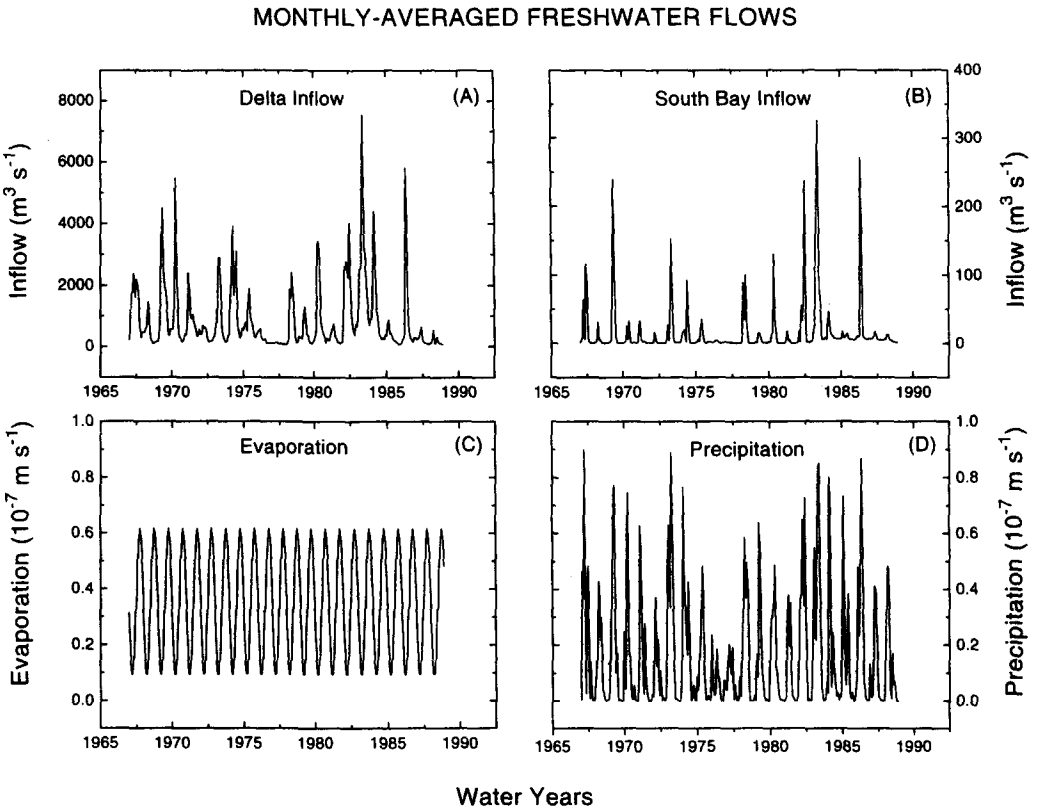

Fig. 2. Observed, monthly averaged freshwater flows to the Bay for water years 1967–1988: (a) Delta inflow (m^3 s^{-1}); (b) South Bay inflow from the Coyote, Guadalupe and Alameda Creeks (m^3 s^{-1}); (c) evaporation rates (taken to be annually repeating in the absence of long-term measured data for the period, units of 10^{-7} m s^{-1}; (d) precipitation rates (units of 10^{-7} m s^{-1}).

Fig. 1. Location charts: (a) chart of San Francisco Bay showing dredging areas (---), bathymetry relative to mean lower low water (—, m), names of major geographical features and the location of the Farallon Islands; (b) chart of San Francisco Bay showing in-plan model segmentation and numbering, long-term Stas 1–7 (•) and major freshwater inflows: A—Napa River, B—Sacramento River, C—San Joaquin River, D—Alameda Creek, E—Coyote Creek and F—Guadalupe Creek. The model Bay comprises the South (1–18) and North (20–45) Bay Branches (SBB and NBB) and the Golden Gate Branch (46–51, GGB). Segment numbers 19 and 51 refer to the same segment.

occurred during the beginning of the last drought in California, between May 1986 to the end of the record in September 1988, when the mean inflow was 210 $m^3 s^{-1}$. The South Bay inflow (Fig. 1) drains a much smaller watershed and its mean over the 22-yr period was 17 $m^3 s^{-1}$, or 2% of the average Delta inflow [Fig. 2(b)]. Periods of high inflow in South Bay generally coincided with those in the Delta.

Measurements of rates of evaporation for the Bay were not made on a regular basis over the period. Because of this, an average annual cycle of evaporation was used for input to the salinity model [Fig. 2(c)]. Minimum and maximum estimated evaporation rates of 0.95 $\times 10^{-8}$ m s^{-1} (12 $m^3 s^{-1}$, using a Bay surface area of 1.24×10^9 m^2) and 6.2×10^{-8} m s^{-1} (77 m^3 s^{-1}), occurred during December and July, respectively [Fig. 2(c)]. The mean evaporation rate was 3.5×10^{-8} m s^{-1} (43 $m^3 s^{-1}$).

Measurements of daily precipitation were available for the 22-yr period. Maximum and minimum precipitation occurred during winter and summer, respectively. Monthly averaged rather than daily averaged precipitation data are plotted in Fig. 2(d) in order to smooth the data for presentation. Daily precipitation rates maximized at 1.2×10^{-6} m s^{-1} (1500 $m^3 s^{-1}$) during December 1981 and the mean rate of precipitation was 1.7×10^{-8} m s^{-1} (21 m^3 s^{-1}). The daily precipitation was often zero. Therefore, on an annual basis, estimated evaporation exceeded precipitation over the Bay by 1.8×10^{-8} m s^{-1} (22 m^3 s^{-1}). During midsummer, estimated evaporation typically exceeded precipitation by 5.7×10^{-8} m s^{-1} (71 $m^3 s^{-1}$). This indicates that, apart from any flushing to the coastal sea, a loss of fresh water from the Bay often occurred during periods of very low freshwater inflow in the summer months of 1976, 1977 and 1987, 1988.

2.2. *Tides and salinity*

Low water and high water within the Bay occur twice each 24.84-h day. The strong diurnal component along the west coast produces large differences between successive low-water and high-water levels. Water circulations are largely driven by Pacific tides that propagate through the Golden Gate (Walters *et al.*, 1985). Surface elevation amplitudes at the Golden Gate, i.e. half the range in water level fluctuations, are M_2 (0.58 m), K_1 (0.37 m) and O_1 (0.23 m). Tidal current-speed amplitudes generally are strong but vary greatly throughout the Bay. M_2 current-speed amplitudes at the Golden Gate exceed 1 m s^{-1} (Walters *et al.*, 1985). In the South and North Bays, M_2 current speeds generally are less than 0.8 m s^{-1} and show a marked reduction in shallower water depths (Cheng and Gartner, 1985; Cheng *et al.*, 1993). Spring–neap variations in tidal currents within the Bay are very pronounced. Over the 22-yr period covering water years 1967–1988, maximum spring tides (1.55 times the mean amplitude at Golden Gate) occurred during December of 1968 and 1986. Minimum neap tides (0.58 times the mean amplitude) occurred during January of 1967 and 1985.

The salinity model requires input data on daily, near-bed salinity in the coastal sea. The seaward boundary of the model was arbitrarily chosen to be 9 km seaward of the Golden Gate [Fig. 1(b)]. As observed salinity data were not available at this boundary, these data were approximated by substituting in their place a 22-yr time-series of monthly (interpolated and resampled to daily) surface salinity data at the Farallon Islands, 50 km offshore of the Golden Gate [Fig. 1(a)]. Although necessary, this substitution was not ideal because of the physical separation of the sites. The mean Farallon Islands salinity over the 22-yr period was 33.4, with maximum values occurring during the summer months and minimum

values during winter [Fig. 3(a)]. Maximum salinity at the Farallon Islands (34.1) occurred during August 1972 and the minimum (28.8) during January 1984.

Salinity data for the seven observational stations [Fig. 1(b)] were derived from two sources. At Sta. 1 (Fort Point, close to the Golden Gate) and Sta. 2 [Alameda, South Bay; Fig. 1(b)], observations were from daily (almost random) surface samples (National Ocean Service, formerly U.S. Coastal and Geodetic Survey, unpublished data). Accuracy of these data is unknown but is estimated to be 0.5. Monthly averages were constructed for these two stations [Fig. 3(a),(b)]. At the other five stations: Stas 3–7 [Martinez, Port Chicago, Pittsburg, Collinsville and Antioch; Fig. 1(b)], salinity was derived from the monthly means of daily averaged (15 min sampling interval) electrical conductivity data (S. Baughman and M. Feris, U.S. Bureau of Reclamation, unpublished data). Mean monthly electrical conductivity was converted to mean monthly salinity using logarithmic regressional calibrations for each station [Fig. 3(b)–(d)].

Relatively few data are available on salinity stratification. However, Smith *et al.* (1991) showed that the maximum intratidal salinity stratification over a spring-neap cycle near the San Pablo Bay entrance to Carquinez Strait [Fig. 1(a)] ranged from about 1–3 during the spring tides to about 9 during the neap tide. Intense stratification could rapidly develop (within a day) during very weak neap tides. Tidally averaged stratification (the mean

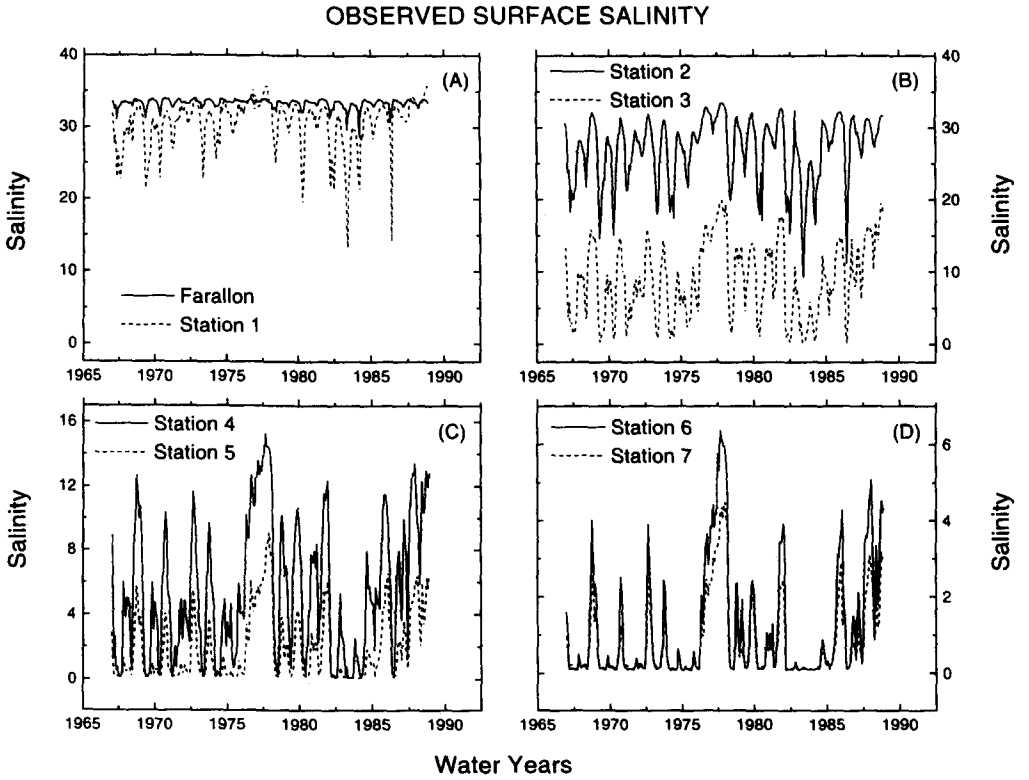

Fig. 3. Observed, monthly averaged surface salinity for water years 1967–1988: (a) Farallon Islands (—) and Sta. 1 (---); (b) Stas 2 (—) and 3(---); (c) Sta.4 (—) and 5(---); (d) Sta. 6 (—) and 7 (---).

stratification over a tidal cycle) was, of course, smaller than the observed maximum stratification during a tide.

Less information is available for the long-term behaviour of salinity in South Bay, although considerable quantities of shipboard survey data are available for primary productivity and salinity (Cloern, 1984, 1987, 1991a,b). The indications are that South Bay, away from both freshwater inflows at the southernmost tip of the Bay and the confluence with North Bay, generally is vertically well mixed for salinity during periods of low freshwater inflow and has low longitudinal density gradients. However, significant stratification can develop during periods of high freshwater inflows and neap tides.

2.3. *Tidally averaged currents*

The long-term salinity model simulates residual (tidally averaged) currents and tidally averaged salinities. Estimates of residual currents, derived from current-meter measurements within North Bay, have been presented by Walters and Gartner (1985) and Smith *et al.* (1991). Walters and Gartner (1985) used data from conventional current meters deployed in Suisun Bay [Fig. 1(a)] to demonstrate the occurrence of gravitational (density-driven) residual currents and their variations within the spring–neap cycle. The gravitational circulation was stronger during neap tides. Residual current speeds were typically 0–0.1 m s^{-1}. Walters and Gartner (1985) also showed that the residual currents were controlled locally by freshwater inflows.

Smith *et al.* (1991) used data from an acoustic Doppler current meter (ADCP) deployed near the San Pablo Bay entrance of Carquinez Strait [Fig. 1(a)]. During neap tides, analysis of the ADCP data revealed near-bed, up-estuary-directed residual currents of magnitude 0.06–0.08 m s^{-1} and near-surface, down-estuary-directed residual currents of magnitude 0.1–0.2 m s^{-1}. During spring tides, the gravitational circulation was reduced and masked by tidally induced residual currents.

Little is known about the long-term gravitational circulation in South Bay. Longitudinal density gradients generally are low during low inflows. Therefore, presumably, South Bay has only weak and variable gravitational circulations at those times.

3. THE LONG-TERM SALINITY MODEL

3.1. *Outline of model*

The three branches of the model Bay comprise 51, two-level segments [Fig. 1(b)]. The South Bay Branch (SBB) is represented by segments 1–18, the North Bay Branch (NBB) by segments 20–45 (with segments 42–45 representing the Delta) and the Golden Gate Branch (GGB, the coastal sea to the confluence of the South and North Bays) by segments 46–51. Segment numbers 51 and 19 refer to the same segment. This segment acts as a node for the three branches of the model Bay.

The upper level of each segment has the same thickness throughout the Bay and the lower level extends to the maximum depth of the segment (Fig. 4). Choosing a constant upper-level thickness simplifies the treatment of longitudinal salinity gradients in the upper level and allows reasonable approximations to be made of the surface salinity in relatively deep areas such as the Golden Gate. The upper level thickness can be altered for any particular simulation, but was maintained at 5 m for the simulations presented in this paper. Salinity is assumed to be uniformly mixed within each of the two levels of a

segment. The salinity and residual circulation throughout the Bay are computed every time step of a simulation, using a time step of one solar day.

Twenty-two years of daily boundary conditions and daily driving environmental variables were needed for a full simulation. Boundary conditions were as follows: salinity of Delta and other inflow waters was zero and salinity was zero at the Delta (segment 45). At the head of South Bay (segment 1) a salinity inflow regression relationship was used to define daily averaged salinity as a function of the low inflows there (Hager and Schemel, in press; Schemel and Hager, in press). The lower-level salinity in segment 46 was taken to be the surface salinity at the Farallon Islands [Fig. 1(a) and Fig. 3(a)]. Daily precipitation and evaporation were taken to be uniformly distributed over the Bay's surface area [monthly averaged data shown in Fig. 2(c),(d)]. Daily freshwater inflow from the Delta [monthly averaged data shown in Fig. 2(a)] entered the model Bay at segment 45, inflow from the Guadalupe and Coyote Creeks at segment 1, inflow from the Napa River at segment 29 and inflow from Alameda Creek at segment 8 [Fig. 1(b)]. Although winds are ignored they could be incorporated at a later stage.

Initial conditions at the start of water year 1967 were taken to be the simulated salinity field at the end of water year 1967. Repeating the simulation several times for 1967,

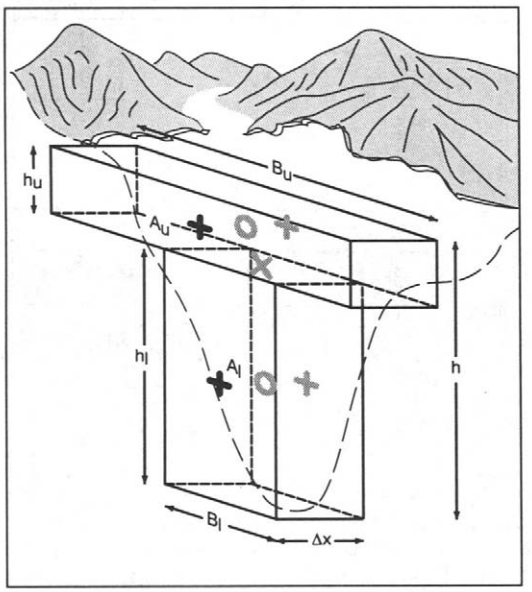

Fig. 4. Schematic of a model Bay salinity segment. The near-surface, upper (u) level of each segment has a fixed depth $h_u = k$ (taken to be 5 m here) and the lower (l) level has a depth h_l which extends between the interface (i) with the upper level to the deepest part of a segment's estuarine section. The vertical faces of the upper and lower levels have cross-sectional areas A_u and A_l, which are equal to the areas of the Bay's estuarine section between the surface and depth h_u and between h_u and the deepest part of the estuarine section, h ($h = h_u + h_l$) at that location. The upper and lower levels of a segment have widths B_u and B_l ($B_u = A_u/h_u$ and $B_l = A_l/h_l$). Salinity is uniformly mixed within each level of a model segment. However, it is useful to think of each level as comprising a salinity node (o) at its centroid and longitudinal velocity nodes (+) either side, in the centres of each vertical cross-sectional face. A vertical velocity node (×) can also be considered to exist in the interface (i) between levels.

starting with a "guessed" solution for salinity and using the final salinity of 1967 as the "start up" salinity for the next simulation of 1967, led to a reasonable initial distribution for the 22-yr simulation.

As a measure of the spring–neap tidal influence on the Bay, the 22-yr record of detrended, hourly hindcasted, Golden Gate water level variations for the simulation period was squared, tidally low pass filtered (using a 25 hr running mean) and then square-rooted to provide the root-mean-square (RMS) water levels for each hour of the record. Averaging the RMS water levels over each solar day and dividing by the average value over the 22-yr record defined the spring–neap tidal state, *TS*, which provided a measure of the relative, spring–neap strength of the Golden Gate tide during each solar day of a simulation.

The model Bay's response to the boundary conditions, freshwater inflows and evaporative outflows depended on the vertical and longitudinal mixing within and between segments (Fig. 5). The mixing, in turn, depended on tidal state, *TS*, and residual current

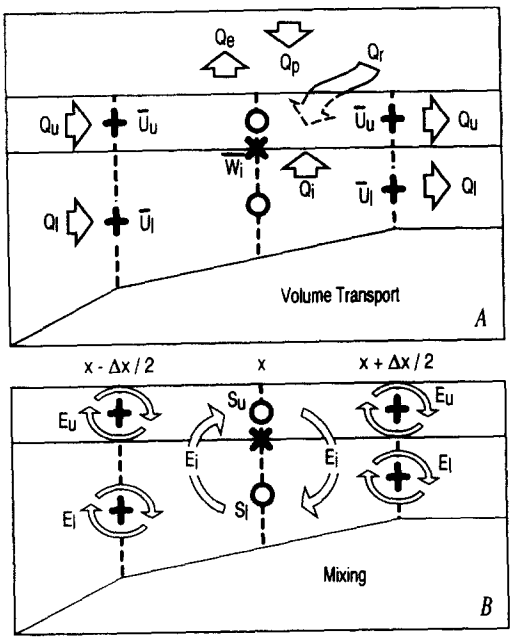

Fig. 5. Schematic of a side view of a model salinity segment: (a) The rate of horizontal flow of water volume through the cross-sectional faces of the upper and lower levels of a segment are $Q_u = A_u\bar{U}_u$ and $Q_l = A_l\bar{U}_l$, where $\bar{U}_u$ and $\bar{U}_l$ are the upper and lower level averaged horizontal velocities defined at (+) nodes. The total rate of flow through a segment's vertical face is $Q = Q_u + Q_l$, so that the longitudinal (x) difference in Q between neighbouring segment faces is $\Delta Q = Q_r + Q_p - Q_e$, where Q_r, Q_p and Q_e are the rates of water volume input to the upper level of segment due to local river inflow, precipitation and evaporation, respectively. The rate of vertical flow of water volume through the interface between upper and lower levels is $Q_i = A_i\bar{W}_i$, where A_i is the interface area and $\bar{W}_i$ the interface averaged vertical velocity, defined at (×) nodes. In the lower level $\Delta Q_l = -Q_i$ and in the upper level $\Delta Q_u = \Delta Q + Q_i$; (b) There are additional, equal and opposite water volume exchanges between the upper and lower levels and between segments which represent mixing processes. E_i denotes the rate of water volume exchange across the interface between upper and lower levels of a segment and E_u and E_l the corresponding longitudinal exchanges between neighbouring upper levels and neighbouring lower levels, respectively.

speeds for each day of a simulation. Within the salinity model, tidal current speeds were tabulated as functions of TS. They were computed from several simulations of a depth averaged, hydrodynamic, numerical model of the Bay. Each run of the hydrodynamic model simulated a different TS, from very weak neap tides ($TS < 1$) to very strong spring tides ($TS > 1$).

3.2. *Basic equations*

Officer's (1976) analysis of gravitational circulation is extended to describe the horizontal residual circulation in the upper (u) and lower (l) levels of each segment of the model Bay (Fig. 4). The momentum equation for the width averaged, longitudinal residual currents within each segment layer is [e.g. the simplified form of equation (3) from Perrels and Karelse (1982) and Proudman (1953), pp. 135–153]:

$$B\partial P/\partial x = \partial(\rho BN\ \partial U/\partial z)/\partial z \tag{1}$$

where P is the hydrostatic pressure, ρ water density, B width (constant in each layer of a segment), N vertical eddy viscosity, U horizontal residual velocity, x horizontal coordinate and z vertical (depth) coordinate. Time dependence has been ignored here so that the residual currents are always in equilibrium with the driving forces.

The upper level of each segment extends from $0 \leq z \leq k$ and the lower level from $k \leq z \leq h$, with $k = 5$ m in this paper. The instantaneous, longitudinal surface slope ($\partial\varsigma/\partial x$) is constant throughout a segment and the instantaneous longitudinal density gradient (λ) is constant within, but different between, both levels of a segment.

Writing the longitudinal pressure gradient in terms of its barotropic and baroclinic parts for the upper level gives:

$$B_u\partial P_u/\partial x = B_u g(\lambda_u z - \rho_u i_u) = \partial(\rho_u B_u N_u \partial U_u/\partial z)/\partial z \tag{2}$$

with:

$$i_u = -\partial\varsigma/\partial x \tag{3}$$

and

$$\lambda_u = \partial\rho_u/\partial x. \tag{4}$$

A condition of zero wind stress is applied at the surface:

$$\rho_u B_u N_u \partial U_u/\partial z|_0 = 0. \tag{5}$$

Writing the longitudinal pressure gradient in terms of its barotropic and baroclinic parts for the lower level gives:

$$B_l\partial P_l/\partial x = B_l g(\lambda_l z - \rho_l i_l) = \partial(\rho_l B_l N_l \partial U_l/\partial z)/\partial z \tag{6}$$

with:

$$i_l = (\rho_u/\rho_l)[i_u - k(\lambda_u - \lambda_l)/\rho_u] \tag{7}$$

and:

$$\lambda_l = \partial\rho_l/\partial x \tag{8}$$

and where the seabed condition is applied:

$$\rho_l B_l N_l \partial U_l / \partial z|_h = -\rho_l \phi_l B_l U_l(h) \tag{9}$$

in which ϕ_l is a drag function derived from linearization of the quadratic drag law.

The longitudinal velocity and the longitudinal frictional force per unit length of a segment must be uniquely specified at the interface between upper and lower levels of a segment, $z = k$:

$$U_u(k) = U_l(k) \tag{10}$$

and

$$\rho_l B_l N_l \partial U_l / \partial z|_k = \rho_u B_u N_u \partial U_u / \partial z|_k + \rho_u \phi_u (B_u - B_l) U_u(k). \tag{11}$$

In order to investigate the sensitivity of the model to vertical and horizontal mixing, Uncles and Peterson (1995) used a no-slip condition at the main channel bed ($\phi_l \rightarrow \infty, U_l(h) = 0$) and a free-slip condition in the upper level ($\phi_u = 0$). This avoided the need to specify the additional environmental variable ϕ while allowing bed friction to be transferred to the upper level via vertical exchange of longitudinal momentum across a segment's interface.

The longitudinal surface slope ($\partial \varsigma / \partial x$) is derived from a knowledge of the rate of water volume transport across a segment's vertical cross-sectional faces:

$$A_u \bar{U}_u + A_l \bar{U}_l = Q \tag{12}$$

where A_u and A_l are the cross-sectional areas of the upper- and lower-level vertical sections, the overbars denote an average over these areas, and Q is the total rate of water volume transport through a segment's vertical face. Except in the specification of density gradients we put $\rho_u = \rho_l = \rho$ and approximate the vertical eddy viscosity by $N_u = N_l = N$. The drag function is approximately by $\phi_u = \phi_l = \phi$, which, in the linearized case, is defined by:

$$\phi = 2C_D\left(\frac{2}{\pi}\bar{U}_T\right)$$

where $\bar{U}_T$ is the amplitude of the depth averaged tidal current velocity, derived from a separately run, depth integrated, hydrodynamic model and $C_D = 2.5 \times 10^{-3}$ (Proudman, 1953). This linearized relationship is valid when the residual currents are much less than the tidal current amplitudes. In the model, a numerical procedure is used to compute ϕ that is valid when residual and tidal currents are comparable (e.g. during high inflow conditions near the Delta).

Level averaged velocities can be derived algebraically by defining the variables:

$$a_1 = 1 + (h - k)\phi / N$$

$$b_1 = 1 - (B_u / B_l)$$

$$a_{21} = \tfrac{1}{6}(\mathbf{g}/\rho N)[\lambda_l (h - k)^2 (2h + k) - \lambda_u k^3 + 3k(\lambda_u - \lambda_l)(h - k)^2]$$

$$a_{22} = -\tfrac{1}{2}\mathbf{g}h(h - 2k)/N$$

$$b_{21} = -(\mathbf{g}/\rho\phi)[(\lambda_u - \lambda_l)(h - k)k + \tfrac{1}{2}\lambda_l (h^2 - k^2) + \tfrac{1}{2}\lambda_u k^2 (B_u / B_l) - \tfrac{1}{6} b_1 \lambda_u k^3 \phi / N]$$

$$b_{22} = \mathbf{g}[(h - k b_1)/\phi - \tfrac{1}{2} b_1 k^2 / N]$$

$$c_1 = (b_{21} + b_1 a_{21})/(1 - a_1 b_1)$$

$$c_2 = (b_{22} + b_1 a_{22})/(1 - a_1 b_1)$$
$$d_1 = (a_{21} + a_1 b_{21})/(1 - a_1 b_1)$$
$$d_2 = (a_{22} + a_1 b_{22})/(1 - a_1 b_1)$$
$$c_3 = c_1 + i_u c_2$$
$$d_3 = d_1 + i_u d_2$$

The level averaged longitudinal velocities are then:

$$\bar{U}_l = c_3[1 + \tfrac{1}{2}\phi(h - k)/N] + \tfrac{1}{24}(h - k)^2(\mathbf{g}/\rho N)\{\lambda_l(3h + k) - 4\rho i_u + 4k(\lambda_u - \lambda_l)\} \quad (13)$$

and:

$$\bar{U}_u = \mathrm{d}_3 + \tfrac{1}{24}k^2(\mathbf{g}/\rho N)(k\lambda_u - 4\rho i_u) \quad (14)$$

where the surface slope is:

$$i_u = -(\partial\varsigma/\partial x) = r/s \quad (15)$$

with:

$$r = Q - e \quad (16)$$

in which:

$$e = A_u\{d_1 + \tfrac{1}{24}gk^3\lambda_u/(\rho N)\} + A_l c_1\{1 + \tfrac{1}{2}\phi(h - k)/N\} + \tfrac{1}{24}A_l(h - k)^2(\mathbf{g}/\rho N)\{\lambda_l(3h + k) + 4k(\lambda_u - \lambda_l)\}$$

and where:

$$s = A_l[c_2\{1 + \tfrac{1}{2}\phi(h - k)/N\} - \tfrac{1}{6}(\mathbf{g}/N)(h - k)^2] + A_u[d_2 - \tfrac{1}{6}\mathbf{g}k^2/N]. \quad (17)$$

A mixing model is used which is analogous to the usual advection-dispersion equation for a continuous (non-discretized), width averaged estuary:

$$\partial(BS)/\partial t = -\partial(BUS)/\partial x - \partial(BWS)/\partial z + \partial(BD\partial S/\partial x)/\partial x + \partial(BK\partial S/\partial z)/\partial z. \quad (18)$$

The righthand side is the sum of advection and mixing. The mixing coefficient K is the vertical eddy diffusivity and D is the coefficient of longitudinal dispersion, which is taken to be the same for both upper and lower levels of a model segment. Integrating equation (18) over the thickness and length of the upper level of a segment gives an equation expressed in terms of the rate of change of the total mass of salt in the upper level (e.g. Uncles, 1988):

$$d(A_u(x)\Delta x S_u(x))/dt = Advection + Mixing \quad (19)$$

with longitudinal and vertical volumetric mixing (or exchange) coefficients (units $m^3\ s^{-1}$; Fig. 5), respectively:

$$E_u = \alpha_u A_u D/\Delta x \quad (20)$$

and:

$$E_i = \alpha_i A_i K/\Delta z \quad (21)$$

with $\Delta z = \frac{1}{2}h(x)$ and where $E_u, E_i > 0$ with subscript i denoting the interface between upper and lower levels of a segment. The quantities α_u, α_i are time independent "constants" over the Bay which, nevertheless, can be altered from unity, if required, to take into account the possibility that the degree of mixing required by the model may differ from that deduced on physical grounds for the real Bay (as specified by D and K). A similar mixing equation for S_l applies to the lower level of a segment by putting $u \rightarrow l$. Diffusivity coefficients N and K are functions of the gradient Richardson Number (Munk and Anderson, 1948). An estimate of the longitudinal diffusivity coefficient, based on formulae and parameter values in Fischer *et al.* (1979, p. 242) is:

$$D = 10^3 \left(\frac{2}{\pi} \bar{U}_T \right)^2 \tag{22}$$

4. RESULTS

Results are described in four subsections. The first deals with a comparison of observed and modelled data. A 22-yr simulation of salinity covering water years 1967–1988 is compared with observed, monthly averaged surface salinity at seven stations [located in Fig. 1(b)]. Daily simulated salinity data at Sta. 5 in the upper reaches of North Bay [Pittsburg in Fig. 1(b)] are compared with observed daily averaged data during water years 1967–1978. This latter comparison demonstrates the ability of the model to simulate very low values of salinity. In the second subsection the location of the modelled FSI is investigated as a function of Delta inflow. The model is used to investigate predicted stratification within the Bay in the third subsection. Finally, the temporal responses of the model Bay to perturbations in coastal salinity and Delta inflow are examined.

The factor α_i multiplying the physically based vertical eddy diffusivity K is 1 without calibration [equation (21)]. To reproduce the fairly strong salinity stratification observed in the Bay, α_i has a value of 0.15 here. The deviation of this factor from unity is probably a consequence of attempting to model vertical processes with just two levels. The factor multiplying the physically based longitudinal eddy diffusivities D in the upper and lower levels ($\alpha_u = \alpha_l$) is 1 without calibration [equation (20)]. To provide for the greater observed mixing in the Bay, α_u and α_l have a value of 1.3 here. In the model version investigated by Uncles and Peterson (1995), $\alpha_u = \alpha_l = 1.1$ and $\alpha_i = 0.25$. Better agreement between simulations and observations could be obtained by allowing α_u, α_l and α_i to vary spatially, but this was not done for the calculations discussed in this article.

4.1. *Observed and modelled data*

The observed salinity at Stas 1–7 (Fig. 3) had strong seasonal signals, which were associated with seasonal variability in freshwater inflows (Fig. 2). At Stas 3–7 the water was sometimes fresh during periods of strong freshwater inflows. The salinity data provided an indication of salinity intrusion and thus the location of the FSI.

4.1.1. *Comparison of monthly averaged observed and modelled data.* Modelled and observed, monthly averaged surface salinity showed reasonable agreement at Sta. 1 (Golden Gate) and Sta. 2 (Alameda), the closest stations to the coastal sea [Fig. 6(a),(b)]. There is an indication that the salinity boundary condition adversely limited the modelled,

higher salinity values at Sta. 1 because observed values exceeded 35 [Fig. 3(a)] whereas the constrained coastal values were never allowed to rise above 34.1 [Fig. 3(a)]. Except for the relatively small effects of evaporation, the maximum, modelled salinity within the Bay could not exceed the coastal input values.

At Sta. 2 (Alameda) the observed data ranged between 8 and 33 [Fig. 6(b)]. This station lies within South Bay, which has very low freshwater inflow [Fig. 2(b)]. Therefore, the bulk of fresh water at this site was the result of mixing with North Bay water, which in turn had been derived from down-estuary flushing of Delta inflow water during very high freshwater inflows.

The modelled and observed data at Sta. 3 (Martinez) showed very similar trends but with an offset between them [Fig. 6(c)]. Agreement improved at salinities >15. The model consistently underestimated salinity at this station; for observed salinity less than about 5 the model predicted fresh water. This indicates that the model located the FSI too far down-estuary at high freshwater inflows, or it is possible that lateral effects may be important at Sta. 3 and within Suisun Bay (see Fig. 12 of Smith and Cheng, 1987).

Closer to the head of the North Bay Branch, at the Delta, there are four stations

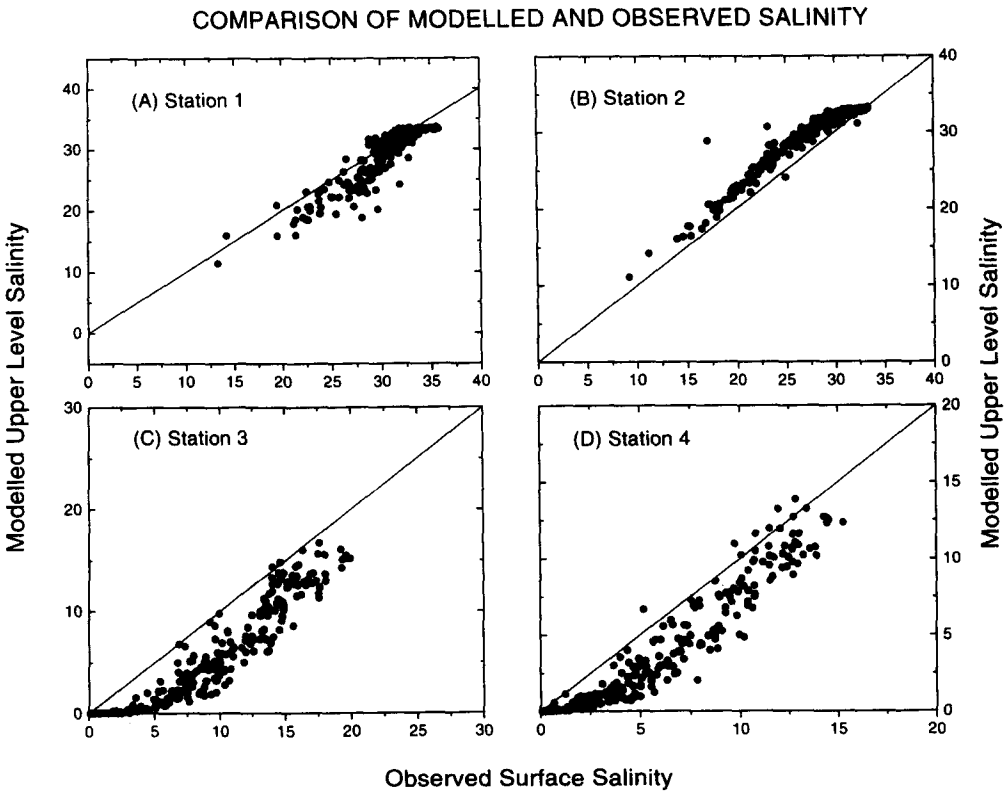

Fig. 6. Comparison of monthly averaged, modelled upper-level salinity (formed from simulated daily data) with monthly averaged, observed surface salinity for water years 1967–1988. The diagonal lines represent a perfect fit between observed and modelled data. Note the changes in scale: (a) Sta. 1 (segment 49, Golden Gate); (b) Sta. 2 (segment 15, Alameda); (c) Sta. 3 (segment 33, Martinez); (d) Sta. 4 (segment 35, Port Chicago).

grouped together: Stas 4–7 (Port Chicago, Pittsburg, Collinsville and Antioch) that are associated with segments 35, 39, 40 and 41, respectively [Fig. 1(b)]. The salinity distributions in this area are sensitive to freshwater inflow and this is reflected in a daily variability in the simulated data (Section 4.1.2). A comparison between modelled and observed, monthly averaged salinity data at Sta. 4 in Suisun Bay [Fig. 6(d)] indicated very similar trends over the salinity range (0–15), although the model again tended to underestimate salinity, especially at high freshwater inflows (salinity <5). The comparisons between modelled data and observed data at Stas 5, 6 and 7 [Pittsburg, Collinsville and Antioch, Fig. 7(a)–(c), respectively] were good over the observed salinity range of 0–10. The results from these latter three stations indicate that the model may be a useful tool for predicting salinity intrusion and the location of the FSI.

A comparison of modelled and observed data at all stations [Fig. 7(d)] indicates reasonable overall agreement; the mean and standard deviation of the modelled minus observed salinity data in Fig. 7(d) are −0.6 (6% of the mean observed salinity for all stations) and 2.0 (17% of the standard deviation of observed salinity for all stations), respectively. If the mean difference between observed and modelled salinity at each

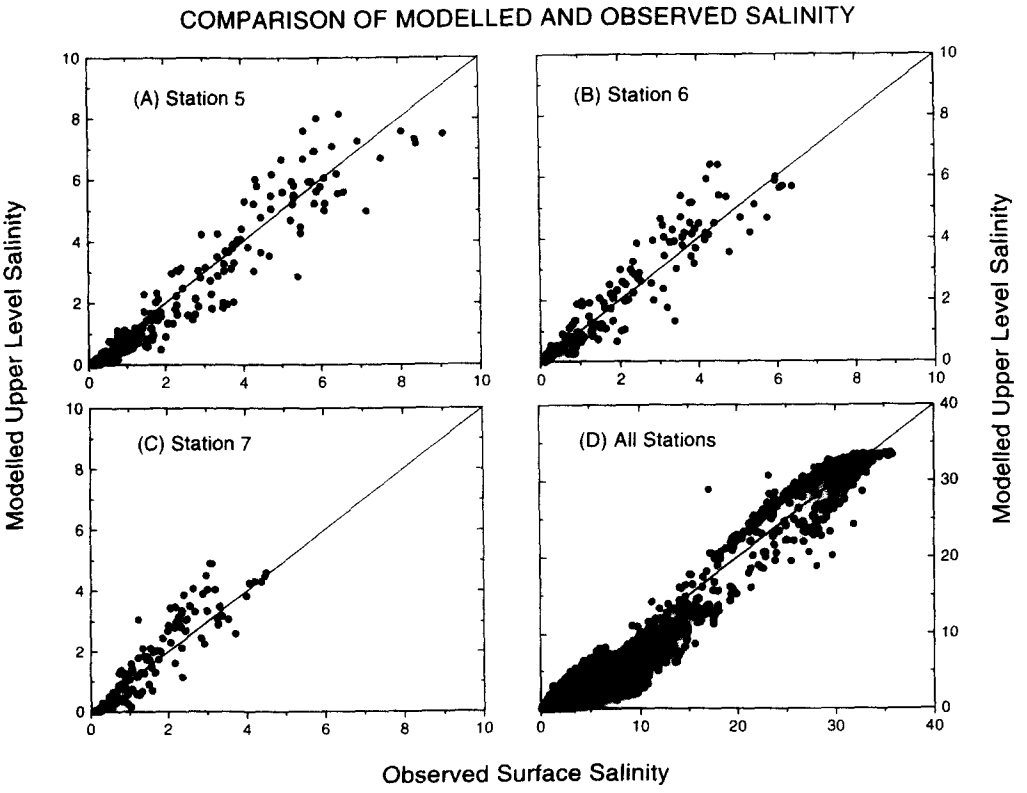

Fig. 7. Comparison of monthly averaged, modelled upper-level salinity (formed from simulated daily data) with monthly averaged, observed surface salinity for water years 1967–1988. The diagonal lines represent a perfect fit between observed and modelled data. Note the changes in scale: (a) Sta. 5 (segment 39, Pittsburg); (b) Sta. 6 (segment 40, Collinsville); (c) Sta. 7 (segment 41, Antioch); (d) all stations pooled.

station is computed and expressed as a percentage of the mean observed salinity at that station, then the mean of the absolute percentages for the seven stations is 14%. If the standard deviation of the difference between observed and modelled salinity at each station is computed and expressed as a percentage of the standard deviation of the observed salinity at that station, then the mean of these percentages for the seven stations is 35%.

4.1.2. *Comparison of modelled and measured daily data.* Daily averaged surface salinity was derived from measurements at Sta. 5 [Pittsburg, Fig. 1(b)] during water years 1967–1978. Excessive gaps occurred in the record after this period. Comparison of daily averaged surface salinity at Sta. 5 with upper-level modelled data indicates close agreement [Fig. 8(a)]. The observed data show a zero offset $\ll 1$, which indicates a systematic instrument error at the lowest salinities. A comparison with daily averaged Delta inflow over the same period [Fig. 8(b)] demonstrates the controlling influence of inflow on near-surface salinity. The model successfully simulated the strong seasonal variability and the effects of the period of very low freshwater inflows during water years 1977 and 1978 (Fig. 8). These results again indicate that the model may be a useful tool for predicting salinity intrusion and the location of the FSI.

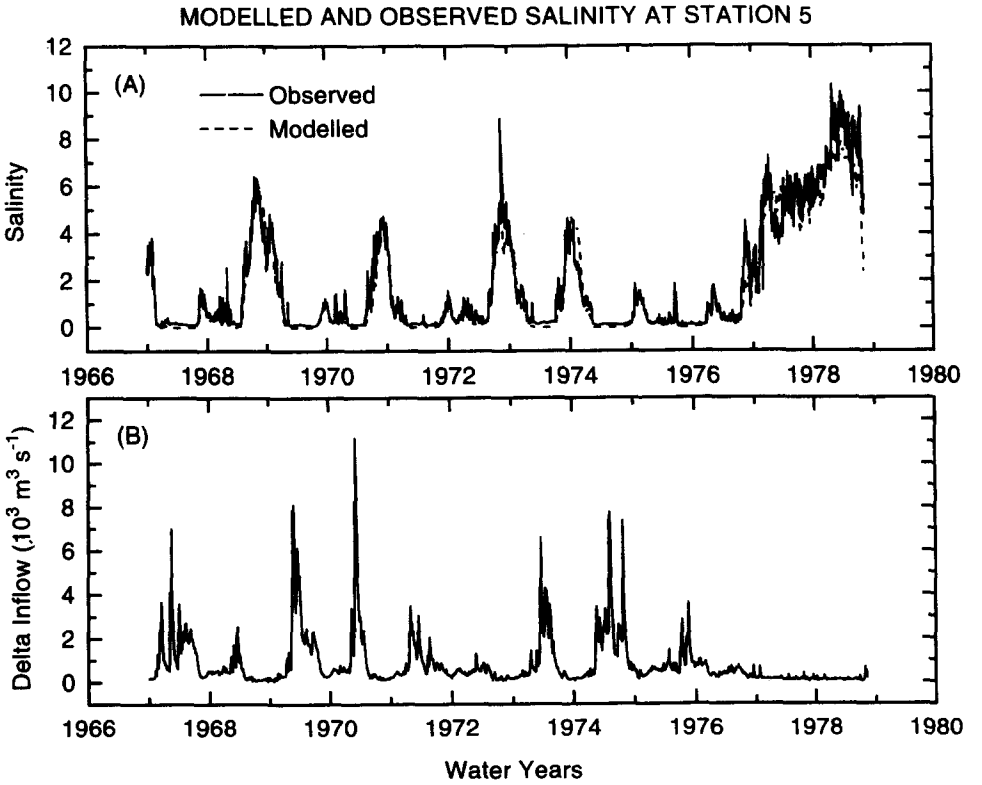

Fig. 8. Comparison of modelled, daily upper-level salinity and observed daily surface salinity at Sta. 5 (segment 39, Pittsburg) and corresponding Delta inflows for water years 1967–1978: (a) measured surface salinity (—) and simulated upper-level salinity (---); (b) Delta inflow ($m^3 s^{-1}$).

A multiple regression analysis of surface salinity at Sta. 5 vs Delta inflow and spring–neap tidal state (*TS*) for the 1977 and 1978 water years, when salinity at Sta. 5 remained non-zero, indicated a strong negative correlation with inflow and a positive correlation with tidal state. Therefore, salinity at Sta. 5 tended to increase with decreasing inflow and with increasing tides.

It is significant that this measure of agreement between model and observations [Fig. 8(a)] was obtained using daily freshwater inflow estimates for the Delta that are known to be approximate. However, recent updates of Delta inflows have been made available to us which incorporate agricultural consumption within the Delta. There is a significant negative correlation (-0.21, $P < 0.001$ with 4108 degrees of freedom) between the daily, agricultural consumption and the salinity residuals (simulated minus observed data from Fig. 8) which provides strong evidence that the model would perform even better with improved flow data.

4.2. *Simulation of the FSI location*

The preferred indicator of saline intrusion in North Bay is the so-called X_2 position, which is the longitudinal location of the 2 isohaline contour 1 m off the bed of the estuary (Kimmerer and Monismith, 1993). Kimmerer and Monismith (1993) used daily averaged, surface salinity data at Stas 3–7 [Fig. 1(b)] and estimated the location of X_2 using interpolation between stations. Two difficulties arose from this procedure; first, the need to estimate near-bed salinity from surface data, and second, the need to fill gaps in the estimated X_2 time-series which resulted both from gaps in the salinity data and from occasions when X_2 was located down-estuary of Sta. 3 (Martinez). Both difficulties were exacerbated at high inflows.

Kimmerer and Monismith (1993) presented estimates of monthly averaged values of X_2 as functions of the logarithm of monthly averaged Delta inflow and showed that the dependence is approximately linear. The simulated values of monthly averaged X_2 estimated from the lower-level salinity of our dynamical salinity model showed pronounced seasonal variability over the 22-yr period, 1967–1988 [Fig. 9(a)]. The simulated, monthly averaged X_2 data showed an approximately linear response to the logarithm of monthly averaged Delta inflow [scatter plot in Fig. 9(b)], in qualitative agreement with the findings of Kimmerer and Monismith (1993). Their results, summarized in terms of a linear regression line, placed X_2 between about 40 and 90 km from the Golden Gate over the range of inflows [continuous line in Fig. 9(b)].

Although the dynamical model agrees with Kimmerer and Monismith's findings at low inflows, there is a discrepancy at high inflows. Dynamically simulated values were located further down-estuary at high inflows and predicted locations were within the range 20–90 km from the Golden Gate. However, it is clear from the comparison of modelled and measured, monthly averaged surface salinity data at Sta. 3 [Fig. 6(c)] that our dynamical model underestimates salinity there. Therefore, because the Sta. 3 data supplied down-estuary conditions for the Kimmerer and Monismith analysis, it is not surprising that results from the two approaches should differ at high inflows.

4.3. *Salinity stratification*

Intratidal mixing processes and tidal straining of the salinity field cannot be resolved in the long-term model, which relies on advection due to modelled gravitational circulation

and vertical mixing to govern the stratification. However, it is useful to investigate the extent to which stratification occurred in the model and to relate this to experimental measurements of stratification and residual currents.

4.3.1. *Bay-wide stratification.* In South Bay the modelled salinity stratification over the 22-yr period was <8 and the modelled, relatively slow gravitational circulation could change direction with increasing Delta inflow. During low inflow conditions the modelled salinity generally increased from south to north in South Bay, owing to freshwater inflows from the Guadalupe and Coyote catchment area [Fig. 10(b)]. However, horizontal salinity gradients were small and gravitational circulations weak away from the creeks. With the onset of strong Delta inflow and low salinity in North Bay, horizontal salinity gradients could reverse in the northern part of South Bay, leading to a salinity maximum there [Fig. 10(a)]. In response, the gravitational circulation could also reverse direction, so that upper-level currents were directed to the south and lower-level currents to the north.

Progressing into North Bay, stratification at the entrance and midway through San

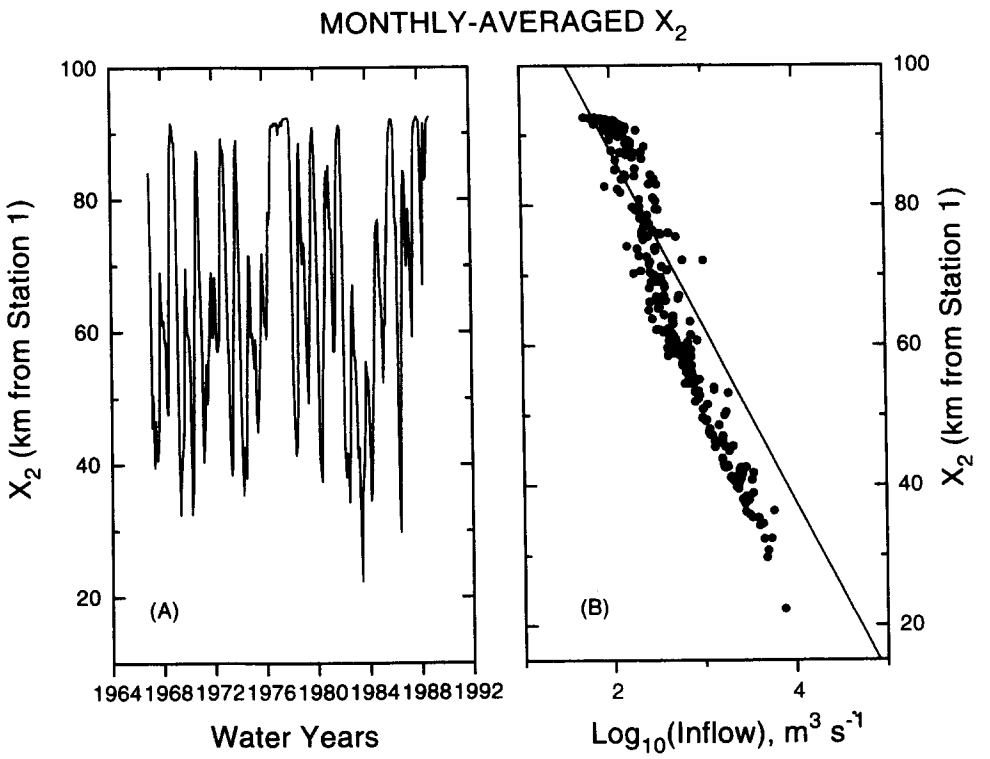

Fig. 9. Location of the monthly averaged, modelled, 2 isohaline in the lower-level of North Bay (X_2) in km relative to Sta. 1 (Golden Gate) during water years 1967–1988 and its relationship to Delta inflow: (a) position of monthly averaged X_2 (km) for water years 1967–1988; (b) modelled, monthly averaged X_2 positions (filled circles, km) as a function of the logarithm of monthly averaged Delta inflow ($m^3 s^{-1}$). The regression line presented by Kimmerer and Monismith (1993) is also shown.

Pablo Bay [segments 22 and 25; Fig. 1(b)] reached maxima of about 10 with increasing freshwater inflow and subsequently decreased as inflow continued to increase. This decrease in stratification at large inflow was the result of reduced upper-level and lower-level salinities as the FSI moved down-estuary and came closer to these sites [Fig. 10(a)]. When inflows exceeded about 3000 $m^3 s^{-1}$, the gravitational circulation was masked by freshwater-induced, down-estuary currents and salinity and stratification rapidly decreased at both these sites.

A similar pattern of modelled stratification and gravitational circulation to that simulated in San Pablo Bay occurred at Stas 3 and 4. However, stratification and gravitational circulation at Sta. 4 were much smaller than at stations further down-estuary because of the shallower depths and lower salinities there. At Stas 5–7 the pattern of modelled stratification differed from that further down-estuary. Stratification and gravitational circulation maximized at the lowest freshwater inflows and were zero when Delta inflow exceeded about 300 $m^3 s^{-1}$ [Fig. 10(b)]. This was a consequence of rapid flushing of salt with increasing inflow.

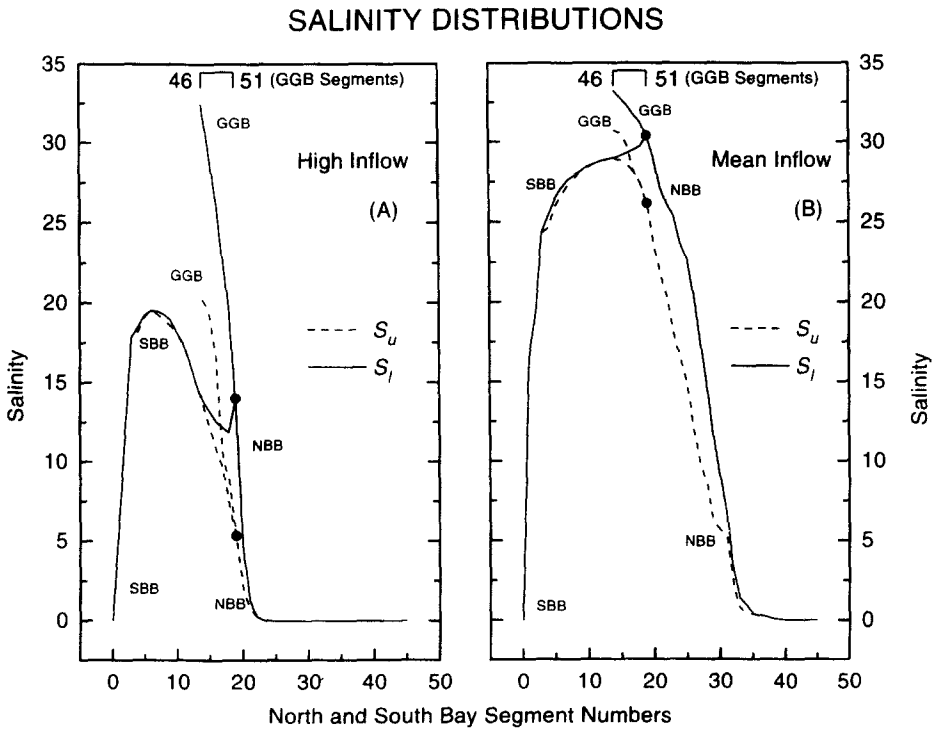

Fig. 10. Simulated upper-level (---, S_u) and lower-level (—, S_l) salinity distributions through the Bay for two occasions of high and average Delta inflows during water years 1967–1988. Salinity is plotted against segment number for the South (1–18) and North (20–45) Bay Branches (SBB and NBB) on the lower horizontal scale and on the upper horizontal scale for the Golden Gate Branch (46–51, GGB). The confluence of the SBB, NBB and GGB at segment 19 (or 51) is highlighted by filled circles: (a) high Delta inflow conditions (8600 $m^3 s^{-1}$) and neap tides (TS = 0.70) on 29 January 1970; (b) mean Delta inflow conditions (800 $m^3 s^{-1}$) and neap tides (TS = 0.64) on 6 February 1972.

4.3.2. *San Pablo Bay stratification.* Smith *et al.* (1991) presented salinity data from near-surface and near-bed at the San Pablo Bay entrance to Carquinez Strait during 16 October–2 November 1986 [segment 29; Fig. 1(b)]. Intratidal variations in stratification were very marked. Neap-tide stratification (near-bed minus near-surface salinity) reached 9 and was much stronger than spring-tide stratification, which was in the range of only 1–3. This spring–neap variation in stratification at the entrance to Carquinez Strait, due partly to the increased vertical mixing during spring tides, also was simulated by the long-term salinity model. High-frequency oscillations in simulated long-term stratification at this site during water year 1988 [the upper line in Fig. 11(a)] were correlated with the spring–neap cycle.

Increasing freshwater inflow enhanced the modelled stratification, both during and for some time after the inflow peaks. Enhanced stratification following peak flows also has been observed in Chesapeake Bay (Boicourt, 1992). However, very strong inflows greatly reduced modelled salinity at the San Pablo entrance to Carquinez Strait so that, for a given spring–neap tidal state, *TS*, the modelled stratification reached a maximum as a function of Delta inflow and thereafter decreased with increasing inflow.

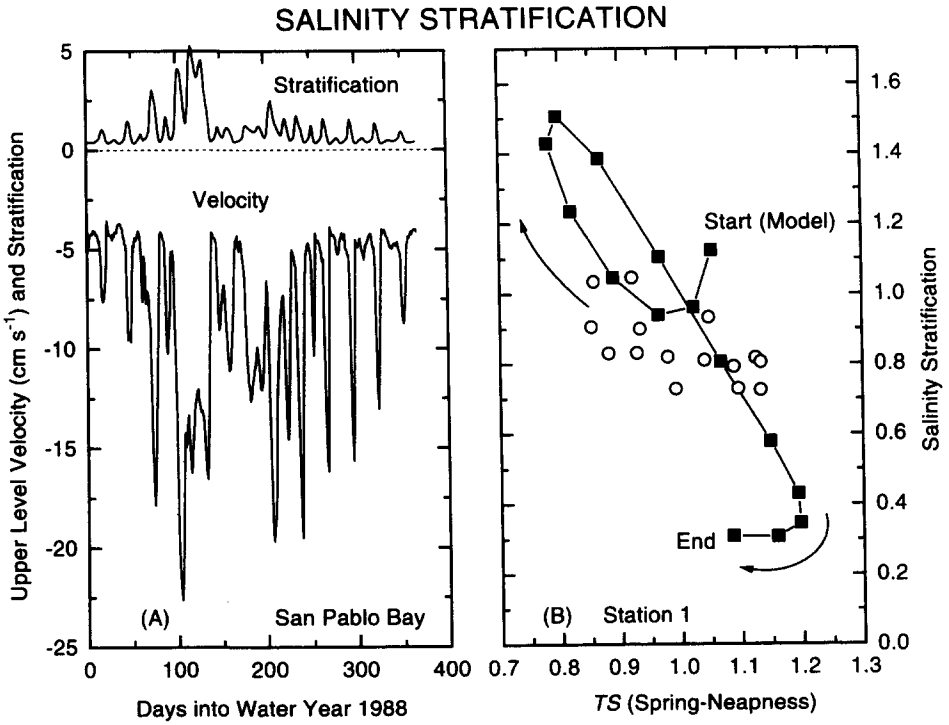

Fig. 11. Modelled, daily stratification and gravitational circulation at segment 29 (the San Pablo entrance to Carquinez Strait) during water year 1988 and modelled and observed, daily stratification at Sta. 1 (segment 49, Golden Gate) during late May and early June of 1980: (a) stratification (upper line, lower-level salinity minus upper-level salinity) and upper-level residual current (lower line, down-estuary flows negative in cm s^{-1}); (b) modelled (■) and observed (○) stratification at Sta. 1 during the same 15-day period, as functions of the relative spring–neapness, *TS*; the arrows indicate a clockwise "rotation" of the modelled stratification from the start of the period at spring tides (*TS* = 1.05) through neap tides (*TS* = 0.81) and back to springs (*TS* = 1.20).

Observed data on the vertical structure of longitudinal residual currents from the San Pablo Bay entrance to Carquinez Strait during May 1988 showed a gravitational circulation with pronounced spring–neap modulations (Smith *et al.*, 1991). The gravitational circulation, deduced by digital, low pass filtering of the instantaneous currents, increased in strength during neap tides. The simulated, daily averaged, upper-level residual current near this site [lower line in Fig. 11(a)] showed similar spring–neap characteristics. Simulated down-estuary currents in the upper level achieved their greatest speeds at times of maximum simulated stratification [Fig. 11(a)]. There was an associated negative correlation between the speed of the simulated gravitational circulation and the spring–neap tidal state (TS).

A linear regression of modelled stratification against modelled, upper-level residual current had a negative correlation [this correlation is visually evident from Fig. 11(a)] and explained 62% of the variance in stratification:

$$\Delta S = -0.4 \pm 0.1 - (18.2 \pm 0.7)\bar{U}_u \tag{23}$$

with $\bar{U}_u$ in m s^{-1}. Therefore, stronger down-estuary residual currents (<0) in the upper level were associated with stronger stratification. A multiple regression of modelled, upper-level currents against inflow (Q) and spring–neap tidal state (TS) explained 65% of the variance in currents. There was a negative correlation with inflow (stronger down-estuary currents with increasing inflow) and a positive correlation with spring–neap tidal state (weaker down-estuary currents with stronger tides):

$$\bar{U}_u = -(183 \pm 7) \times 10^{-3} - (144 \pm 7) \times 10^{-6}Q + (12 \pm 1) \times 10^{-2}TS. \tag{24}$$

The modelled, lower-level currents [equation (13)] were negatively correlated with both spring–neap tidal state and inflow (stronger inflows and tides leading to weaker up-estuary currents). A multiple regression of the modelled, lower-level currents against inflow and tidal state explained 52% of the variance in currents:

$$\bar{U}_l = (75 \pm 3) \times 10^{-3} - (25 \pm 3) \times 10^{-6}Q - (51 \pm 3) \times 10^{-3}TS. \tag{25}$$

A comparison of the modelled, lower-level currents with values predicted by this multiple regression shows large scatter, which indicates the importance of nonlinearities, delays and transients in the response of these currents and stratification to the environmental forcing variables.

There appears to be insufficient measurements to indicate how the gravitational circulation varied experimentally with freshwater inflow (Smith *et al.*, 1991). However, the modelled results for this site showed the reduction of lower-level gravitational circulation during higher inflow and its replacement by a down-estuary flow during the major, high inflow periods.

The modelled, spring–neap control on gravitational circulation at the San Pablo Bay entrance to Carquinez Strait also occurred throughout most of North Bay at moderate freshwater inflows. In particular, it occurred within Suisun Bay, in qualitative agreement with measurements presented by Walters and Gartner (1985). The observed and modelled gravitational circulations were not always continuous throughout North Bay, but could be masked by inflow-induced, down-estuary currents during higher inflows in areas which are particularly shallow (Walters *et al.*, 1985).

4.3.3. *Golden Gate stratification.* Measurements of salinity over a spring–neap cycle were made in the vicinity of Sta. 1 in 97 m of water during late May and early June of 1980.

Recording salinometers were moored at 20 m and 90 m beneath the surface. The observed, tidally averaged stratification (salinity at 90 m minus that at 20 m) had a magnitude which generally ranged between 0.7 and 1.1 during the spring–neap deployment [Fig. 11(b)]. The freshwater inflow decreased over the period and for some time before the deployment, so that stratification tended to decrease with time on time-scales longer than a spring–neap cycle. The mean and standard deviation of Delta inflow over the period were 420 and 30 m^3 s^{-1}. Despite the scatter in observed stratification [open circles in Fig. 11(b)], it is evident that minimum observed stratification occurred during spring tides [$TS>1$ in Fig. 11(b)], with values of TS for the observations defined from simultaneous measurements of tidal currents at Sta. 1 and that maximum stratification occurred during neap tides ($TS < 1$).

The modelled, daily averaged stratification (lower-level minus upper-level salinity) at Sta. 1 showed similar spring–neap behaviour to the observations and was of similar magnitude, with the same mean value. A 15-day period of modelled stratification had a pronounced spring–neap signal, with stratification varying from about 0.3 at springs to 1.5 at neaps [Fig. 11(b)]. The modelled data corresponded to the same time period as the observed data in Fig. 11(b). A feature of the modelled data which is not apparent in the somewhat noisy observed data is the hysteresis in stratification over a spring–neap cycle [illustrated by the elliptical nature and clockwise "rotation" of the modelled stratification in Fig. 11(b)]. For a given spring–neap tidal range, and fairly steady inflows, the stratification was higher progressing from neaps to springs than from springs to neaps.

The modelled stratification at Sta. 1 was strongly dependent on freshwater inflow, as indicated by Delta inflow over the 22-yr period. Modelled stratification was positively correlated with Delta inflow, for inflow which was not too high, and negatively correlated with tidal range. Maximum modelled stratification over the 22-yr period was 13. This occurred during neap tides when Delta inflow was 8600 m^3 s^{-1} [Fig. 10(a)]. The modelled upper-level gravitational circulation also increased with increasing inflow and decreasing spring–neap tidal state. Maximum modelled, upper-level residual current speed was about 0.62 m s^{-1}. Lower-level gravitational circulation tended to increase with increasing inflow (in contrast to most of North Bay) for inflow that was not too high, and with decreasing tidal state. Maximum modelled, lower-level residual current speed was 0.08 m s^{-1}.

4.4. *Bay response time characteristics*

The simulated responses of the Bay to perturbation in coastal sea salinity and Delta inflow provide an indication of the time-scales of salinity variability within the Bay. To investigate these time-scales, simulations have been performed about low inflow, steady-state conditions for both salinity and Delta inflow perturbations.

For salinity perturbations a small, sinusoidal salinity signal with a period of 1 yr was applied at the coastal boundary (Simulation 1) as well as a pulse of salinity with a duration of 1 day (Simulation 2). The time-scale of importance for the sinusoidal salinity perturbation is the time lag between the salinity maximum at any position within the Bay and its maximum at the coastal boundary, T_L. This time lag and the amplitude of the corresponding salinity signal were determined throughout the Bay using Fourier transforms. Two time-scales can be defined for the salinity pulse [Simulation 2; Fig. 12(a)]. The rise time, T_R, at any position in the Bay is the time taken for the peak of the pulse to occur after the peak of the coastal boundary pulse. The fall time, T_F, is the time that it subsequently takes for the pulse to fall by 90% of its peak-to-baseline (BL) height [Fig. 12(a)]. Throughout the

Bay, salinity pulse height can be expressed as a ratio of local pulse height to pulse height at the coastal boundary.

For Delta inflow perturbations a small, sinusoidally varying inflow signal with a period of 1 yr was superimposed on an otherwise constant Delta inflow (Simulation 3) as well as a pulse of inflow with a duration of 1 day (Simulation 4). The responses manifested themselves as small changes in the freshwater fraction, $(1\text{-}S/S_O)$, where S_O is coastal salinity. For the sinusoidal inflow perturbation, time lags, T_L, and signal amplitudes of the freshwater fraction were computed throughout the Bay using Fourier transforms. Timescales T_R and T_F also can be defined for the freshwater fraction pulse [Simulation 4; Fig. 12(b)].

4.4.1. *Salinity perturbations.* A sinusoidal salinity perturbation with a period of 1 yr and an amplitude of 0.5 was applied to the near-bed salinity at the coastal boundary [segment

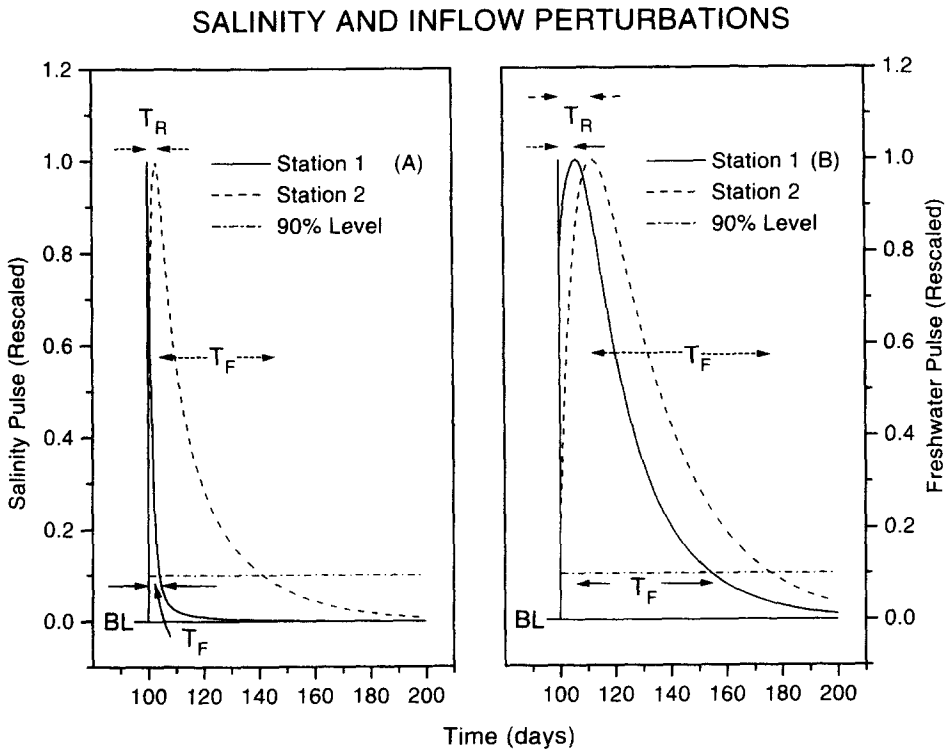

Fig. 12. Normalized response pulse shapes, simulated at Stas 1 (—) and 2 (---) for salinity and Delta inflow perturbations which have been superimposed on steady-state, low inflow summer conditions. Data are plotted against time (days) and perturbations were applied at 100 days into the simulations. The steady-state simulation is shown as baseline (BL) and the 90% return level as the horizontal dash-dot line: (a) the salinity pulse is applied in the lower-level of the coastal boundary and the pulses at Stas 1 and 2 show the rise time (T_R and 90% fall time) (T_F) in days for the lower-level signal responses; (b) the inflow pulse generates freshwater fraction response pulses at Stas 1 and 2 and the rise times(T_R) and 90% fall times (T_F) in days are shown for the upper-level signal responses; rise times for inflow perturbations are extremely fast in the Golden Gate and North Bay Branches (and therefore at Sta. 1) owing to the requirement for inflow volume continuity.

46; Fig. 1(b)] which was otherwise kept at its average value of 33.4 (S_O). The Delta inflow was kept constant at 300 $m^3\ s^{-1}$, corresponding to summer inflows. The tidal range, evaporation and precipitation were maintained at their average levels.

The sinusoidal salinity perturbation propagated into the Bay and its height (twice the amplitude) decayed as it moved into North Bay towards the Delta and down South Bay [Simulation 1; Fig. 13(a)]. The signal height reached 50% of its coastal value at segment 32 (Carquinez Strait) in the North Bay and at segment 3 in the South Bay [Fig. 1(b)]. The "step" on the pulse height in North Bay was located in the San Pablo Bay entrance to Carquinez Strait and reflects the marked change in topography at this location.

The salinity perturbation required about 10 days to propagate from the coastal boundary to the confluence of the South and North Bay Branches. It required about 45 and 40 days to propagate from the coastal boundary to the Delta and to the head of South Bay, respectively [Simulation 1; Fig. 13(b)].

The salinity pulse, applied with a duration of 1 day at the coastal boundary, propagated into the Bay and its amplitude rapidly decayed with distance as it moved into North Bay towards the Delta and down South Bay [Simulation 2; Fig. 13(a)]. The amplitude decreased to about 17% of its coastal boundary value at the confluence of the South and North Bay Branches.

The salinity pulse rise times varied from zero at the coastal boundary to about 30 and 25 days at the heads of the North and South Bay Branches, respectively [Simulation 2; Fig. 13(b)]. The pulse fall times varied from zero at the coastal boundary to about 60 days at the head of North Bay and 65 days at the head of South Bay. The marked decrease in width between San Pablo Bay and Carquinez Strait was highlighted by a "step" in the rise and fall time-scales there [Fig. 13(b)]. Although the choice of a 90% fall time was arbitrary, there is a close similarity between the sinusoidal perturbation lag times (Simulation 1) and the mean of the pulse rise and fall times (Simulation 2).

4.4.2. *Freshwater perturbations*. A sinusoidal inflow perturbation with a period of 1 yr and an amplitude of 10 $m^3\ s^{-1}$ was superimposed on an otherwise constant, summer Delta inflow of 300 $m^3\ s^{-1}$ (Simulation 3). The tidal range, evaporation, precipitation and coastal, near-bed salinity were kept constant at their average values. The inflow perturbation generated freshwater fraction responses through the Bay. These were zero in the freshwater inflows of the Delta and of South Bay (because the freshwater fractions there were unity–zero salinity) and were very small at the coastal boundary [Simulation 3; Fig. 14(a)]. Maximum freshwater fraction responses occurred in the low inflow region of highest horizontal salinity gradients [Fig. 10(b)] between San Pablo and Suisun Bays [Fig. 1(a)].

Throughout North Bay to the coastal boundary, freshwater fraction signals generated by the sinusoidal inflow perturbation maximized between 12 and 21 days after the inflow maximum [Simulation 3; Fig. 14(b)]. That is, within a period of 9 days throughout this region. Lag times, T_L, were a minimum in the low inflow region of high horizontal salinity gradients. The signal required about 50 days in order to maximize at the head of South Bay [Simulation 3; Fig. 14(b)]. This is about 30 days after the signal maximized at the confluence of the South and North Bay Branches, which is consistent with the time lags which occurred in response to a sinusoidal salinity perturbation at the coastal boundary.

The Delta inflow pulse generated a freshwater fraction response throughout the Bay with a pulse height which, relative to its Bay-averaged value, was very similar to that

exhibited by the sinusoidal inflow perturbation [Simulation 4; Fig. 14(a)]. The freshwater fraction pulse rise time was <7 days between the coastal boundary and the head of North Bay [Simulation 4; Fig. 14(b)]. It increased to 35 days at the head of South Bay, consistent with other time-scales there. The 90% fall time varied between 20 and 50 days over North Bay and through to the coastal boundary [Simulation 4; Fig. 14(b)]. The 90% fall time in South Bay increased from 50 to 75 days between the confluence of the South and North Bay Branches and the head of South Bay, corresponding to a 25-day increase over that distance.

5. DISCUSSION

Although the model provides realistic simulations without altering the mixing coefficients from their physical estimates, some degree of calibration can improve the statistical comparisons between modelled and observed data (Uncles and Peterson, 1995). The factor α_i multiplying the vertical eddy diffusivity is 1 without calibration. Modelled

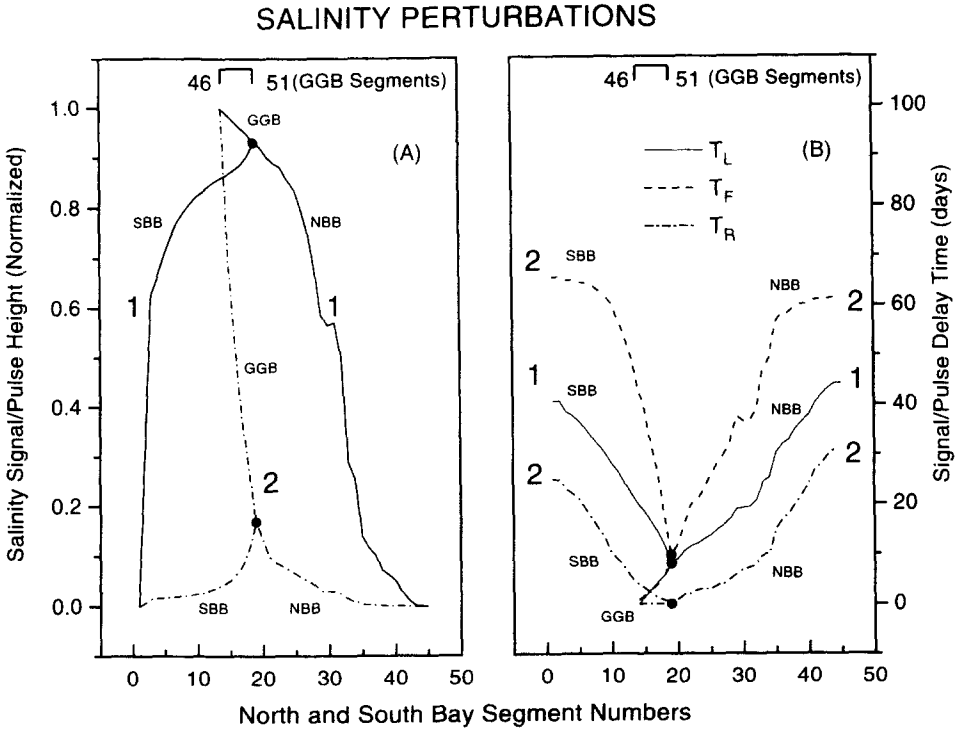

Fig. 13. Heights (or amplitudes) and delay times of salinity responses in the lower level due to sinusoidal and pulsed salinity perturbations applied in the lower level at the coastal boundary. Data are plotted against segment number for the South (1–18) and North (20–45) Bay Branches (SBB and NBB) on the lower horizontal scale and against segment number on the upper horizontal scale for the Golden Gate Branch (46–51, GGB). The confluence of the SBB, NBB and GGB at segment 19 (or 51) is highlighted by filled circles: (a) heights (or amplitudes) of salinity responses relative to the coastal heights (or amplitudes) for the sinusoidal (——, 1) and pulsed (·····, 2) perturbations; (b) time lag (T_L) of the salinity responses to the sinusoidal perturbation (——, 1) and rise time (T_R, ·····, 2) and 90% fall time (T_F, ----, 2) of the salinity responses to the pulsed perturbation.

salinity is fairly insensitive to this factor. The results presented here use $\alpha_i = 0.15$. This small value of α_i is required to reproduce sufficiently strong stratification and is probably a result of replacing the continuous water column with just two levels. When the model transfers water and salinity from the upper to the lower level, and vice versa, the transferred material is immediately mixed throughout the level's volume, thereby effectively enhancing the vertical mixing. The factor α_u multiplying the longitudinal mixing coefficient is 1 without calibration. Modelled salinity is fairly sensitive to this factor. The value used here is $\alpha_u = 1.3$. This factor will depend, in some complex, difficult to define way, on the spatial variability of channel width and coastline shape.

The observed, monthly averaged salinity data at Stas 1–7 exhibited seasonal variability over the 22-yr period which was related to seasonal fluctuations in freshwater inflows. Lower salinity was associated with stronger inflow. The salinity model also demonstrated these features. Using linear time-series analysis, Uncles and Peterson (1995) showed that the inflow response of the simulated salinity is very similar to that exhibited by the

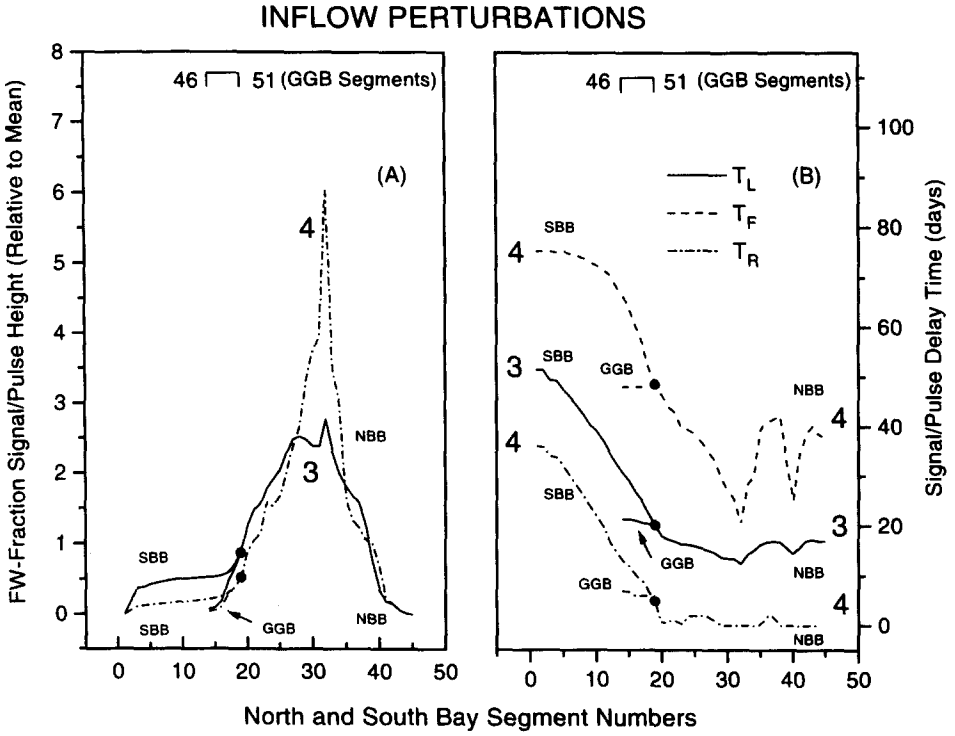

Fig. 14. Heights (or amplitudes) and delay times of freshwater fraction responses due to sinusoidal and pulsed Delta inflow perturbations. Data are plotted against segment number for the South (1–18) and North (20–45) Bay Branches (SBB and NBB) on the lower horizontal scale and against segment number on the upper horizontal scale for the Golden Gate Branch (46–51, GGB). The confluence of the SBB, NBB and GGB at segment 19 (or 51) is highlighted by filled circles: (a) heights (or amplitudes) of freshwater fraction responses relative to the Bay-averaged heights for the sinusoidal (——, 3) and pulsed (·····, 4) perturbations; (b) time lag (T_L) of the freshwater fraction responses to the sinusoidal perturbation (——, 3) and rise time (T_R,·····, 4) and 90% fall time (T_F, ----, 4) of the freshwater fraction responses to the pulsed perturbation.

observed salinity in the seaward reaches of the Bay. Further into the Bay, salinity can be zero during high inflow periods and linear time-series analysis is not then possible.

Modelled and observed surface salinity over the 22-yr period shows reasonable agreement at Stas 1 and 2, the closest stations to the coastal sea. This degree of fit was not a result of boundary constraint on the simulations. Boundary salinity data were limited to the range 28.8–34.1. Observed salinity at Sta. 1 fell as low as 13. The modelled and observed salinity data at Sta. 3 show very similar trends but with an offset of about 3–5 between them. The comparison at Sta. 4 indicates very similar trends over the salinity range (0–15) although the model again tends to underestimate salinity, especially at high freshwater inflows (when salinity <5). Comparisons at Stas 5–7 are good over the observed salinity range of 0–10. The least satisfactory comparisons were at Stas 3 and 4, in the region which has highest horizontal salinity gradients at low inflows.

It is not known why the model supplies poorer comparisons with observed salinity in the central reaches of the North Bay Branch. For the real Bay, lateral effects may be partly responsible, or stronger gravitational circulation in Carquinez Strait during very high freshwater inflows. The model cannot simulate lateral behaviour and is restricted to just two levels in the vertical; spatially averaged salinity is simulated in both these levels. Therefore, if very strong stratification occurs during the highest freshwater inflows through the Strait, the model will not respond correctly to this unless the upper level thickness is the same as the surface layer thickness in the Strait. Ford *et al.* (1990) have presented salinity data for North Bay during very high inflows at high-water slack of a neap tide. Strong stratification occurs, although the 5 m upper-level thickness in the model is similar to the observed layering.

If the mean difference between monthly averaged, observed and modelled salinity at each station is computed and expressed as a percentage of the mean observed salinity at that station, then the mean of these absolute percentages for the seven stations is 14%. This represents a reasonable, Bay-wide simulation of the mean, long-term salinity field. If the standard deviation of the difference between monthly averaged, observed and modelled salinity at each station is computed and expressed as a percentage of the standard deviation of the observed salinity at that station, then the mean of these percentages for the seven stations is 35%. This is larger than one would wish. Fine-tuning of the calibration coefficients and incorporation of spatial dependence would improve the agreement. However, a significant, but unquantifiable part of this percentage difference is undoubtedly due to measurement inaccuracies and sampling deficiencies in the observations themselves, as well as inaccuracies in the experimental estimates of Delta inflow.

At Stas 3–7 the water was sometimes fresh for part of the year, concurrent with strong freshwater inflows. Good simulations are obtained at Stas 5–7. Comparison of daily averaged, observed salinity at Sta. 5 with modelled daily data during water years 1967–1978 indicates a strong measure of agreement at the daily time-scale; the model successfully simulates the marked seasonal variability in salinity as well as the effects of rapidly changing freshwater inflows and the associated migration of the FSI through Sta. 5.

The FSI is an important region in North Bay, not only because it delimits the saline intrusion but also because of its important influence on the ecology of North Bay (San Francisco Estuary Project, 1993) and its association with the gravitational-circulation null zone and turbidity maximum (Conomos and Peterson, 1977; Peterson *et al.*, 1975, 1978; Cloern, 1987). Simulated values of monthly averaged X_2, estimated from lower-level salinity of the long-term salinity model, showed pronounced seasonal variability with an

approximately linear response to the logarithm of monthly averaged Delta inflow. Modelled locations were within the range 20–90 km from Sta. 1 at the Golden Gate. Statistical analyses by Kimmerer and Monismith (1993) computed X_2 to lie between 40 and 90 km from the Golden Gate. Some of the discrepancy in X_2 locations between the two approaches may be due to limitations in their statistical model, while some may relate to the fact that the salinity at 1 m above the estuary's bed will be somewhat greater than that modelled dynamically in the lower level of our salinity model. Another source of discrepancy is the difference between modelled and observed salinity at Sta. 3 (used in the Kimmerer and Monismith analysis) during high inflow.

Stratification also has an important influence on the ecology of the Bay. Cloern (1991a) has shown that the spring bloom is typically associated with density (salinity) stratification of the water column induced by freshwater inflow. Stratification of the water column is dependent upon the dynamical balance between buoyancy and mixing forces. Buoyancy input through freshwater inflow, coupled with advection of fresher water over more saline water due to tidal and gravitational circulation, tends to increase stratification. Vertical mixing through tidally induced shear at the seabed tends to reduce stratification.

Modelled stratification depended strongly on both freshwater inflow and location within the Bay. Salinity stratification was not greatly limited by lack of lower-level salinity in the Golden Gate Branch and stratification tended to increase with freshwater inflow up to very high values. Stratification was severely limited by low, lower-level salinities near the Delta, even for weak Delta inflows ($\sim 300\ m^3\,s^{-1}$).

Strong Delta inflows reduced modelled salinity at the San Pablo entrance to Carquinez Strait. In consequence, the modelled stratification for a given spring–neap tidal state there, and in central North Bay, reached a maximum as a function of Delta inflow and thereafter decreased with increasing inflow. The reduction of salinity to low values resulted in a lower density difference between inflow and estuarine waters, so that vertical mixing and barotropic pressure gradients then dominated the effects of buoyancy. Model results showed the reduction of lower-level gravitational circulation during higher inflow and its replacement by a down-estuary flow during the highest inflow periods.

There was a modelled, spring–neap control on gravitational circulation at the San Pablo Bay entrance to Carquinez Strait which also occurred throughout most of North Bay at moderate freshwater inflows. Simulated down-estuary currents in the upper level were strongest during maximum simulated stratification. There was a negative correlation between the speed of the simulated gravitational circulation and the spring–neap tidal state; larger tides leading to slower gravitational currents. Modelled gravitational circulations were not always continuous throughout North Bay, but could be masked by down-estuary currents during higher inflows in shallower areas.

At the Golden Gate, a 15-day period of modelled stratification had a strong spring–neap signal. Stratification varied from about 0.3 at springs to 1.5 at neaps. An interesting feature of the modelled data is the hysteresis in stratification over a spring–neap cycle, such that for a given spring–neap tidal range, and fairly steady inflows, the stratification was higher progressing from neaps to springs than from springs to neaps. This is because energy was required to remix the water column following neap-tide stratification in the model.

A knowledge of the response of the Bay to perturbations in coastal sea salinity and Delta inflow is useful as an aid to understanding the salinity variability within the Bay and its relationship to local and non-local forcing. A simulated, sinusoidal salinity perturbation at the coastal boundary with a 1-yr period decayed as it moved into the North and South

Bays. The signal reached 50% of its coastal level in Carquinez Strait and at a location close to the head of South Bay. It required about 10 days to propagate from the coastal boundary to the confluence of the South and North Bays and about 45 and 40 days to propagate to the Delta and to the head of South Bay, respectively. However, in South Bay this latter time is a strong function of the assumed, longitudinal mixing coefficients and these cannot be estimated with certainty from salinity data because of the low salinity gradients in South Bay and the lack of long-term data with which to compare model and observations.

A simulated salinity pulse of 1 day's duration at the coastal boundary rapidly decayed with distance as it moved into the Bay and decreased to about 17% of its coastal level at the confluence of the North and South Bay Branches. This strong decay was partly a consequence of the short duration of the pulse. Before reaching the North and South Bay Branches the pulse was partially mixed from lower to upper levels and much of its salt flushed seawards by near-surface gravitational circulation. The pulse rise times increased from zero at the coastal boundary to about 30 and 25 days at the heads of the North and South Bays, respectively, and the pulse fall times increased from zero to about 60 and 65 days there, respectively.

A sinusoidal Delta-inflow perturbation with a period of 1 yr generated freshwater fraction responses which were zero in the freshwater inflows of the Delta and South Bay (because of zero salinity there) and which were very small at the coastal boundary, where salinity changes were minimized by large water volumes and low horizontal salinity gradients. Maximum freshwater fraction responses occurred in the region of highest horizontal salinity gradients (at low inflow) between San Pablo and Suisun Bays. Apart from South Bay, freshwater fraction signals maximized between 12 and 21 days after the inflow maximum. Lag times were a minimum in the low inflow region of high horizontal salinity gradients. The signal required about 50 days to maximize at the head of South Bay, which was about 30 days after the signal maximized at the confluence of the South and North Bay Branches.

A Delta inflow pulse of 1 day's duration generated a freshwater fraction response which was very similar to that exhibited by the sinusoidal perturbation. A much sharper peak in pulse height at the Suisun Bay entrance to Carquinez Strait was a consequence of the important influence of transients in the pulse simulations, in association with the sharp changes in bathymetry of this region. Apart from South Bay, the pulse rise time was <7 days. It increased to 35 days at the head of South Bay. The 90% fall time varied between 20 and 50 days over North Bay and through to the coastal boundary. The shortest fall times occurred in the low inflow region of highest horizontal salinity gradients. The fall time in South Bay increased from 50 to 75 days between the mouth and head of South Bay—a 25-day increase over the region.

The fast rise times in North Bay (and through to the coastal boundary) which resulted from the Delta inflow pulse were a consequence of the fact that the transport consisted of processes which defined three time-scales, two of which were relatively fast. The first and fastest (the depth mean advection due to cross-sectionally averaged water volume transport) was much less than the time step interval of one day. Therefore, down-estuary migration of the isohalines occurred almost immediately (<1 day). The second transport component was due to the down-estuary advection of fresher (but continuously mixed) water in the upper-level gravitational current. The mean current of 0.06 m s^{-1} over a distance, L, of about 80 km between the North Bay FSI and Golden Gate (see Fig. 9 for an inflow of 300 $m^3 s^{-1}$), resulted in a travel time of 15 days. The third time-scale was due to

longitudinal mixing of the pulse from the Delta to the Golden Gate. This time was of the order of $0.4L^2/D$ (Fischer *et al.*, 1979) where D is the longitudinal dispersion coefficient. Using an average, modelled North Bay dispersion coefficient of $D = 130\ m^2\ s^{-1}$ gives a time-scale of roughly 250 days. Therefore, the first two transport processes were responsible for the fast response time of North Bay to fluctuations in inflow.

In the case of salinity perturbations at the seaward boundary, the dominant time-scale in North Bay is determined by up-estuary gravitational circulation in the lower level. This time-scale is $t = L/U_l$ which with $L = 80$ km and $U_l = 0.02\ m\ s^{-1}$ gives $t = 45$ days, which is the same order of magnitude as the modelled response times in North Bay. The slower processes of up-estuary advection in the lower-level gravitational circulation and longitudinal mixing, resulted in slower response times for a salinity perturbation than for a Delta inflow pulse.

If a salinity perturbation is applied at the coastal boundary and thereafter held constant (approximating a slow, seasonal variation) then after a short initial time an appropriate time-scale for diffusive relaxation of perturbed salinity throughout the Bay, δS, is [by analogy with the classical diffusion equation solution of heat distribution along a finite bar of length L (e.g. Smith, 1967)]:

$$\delta S \approx A_1 \exp(-D\pi^2 t/L^2).\sin(\pi x/L). \tag{26}$$

Therefore, using a 90% decay time:

$$t_{90} = 2.3L^2/\pi^2 D. \tag{27}$$

For South Bay, $L = 53$ km and under low inflow conditions $D = 190\ m^2\ s^{-1}$, so that $t_{90} =$ 40 days. For North Bay, $L = 80$ km and $D = 130\ m^2\ s^{-1}$, so that $t_{90} = 130$ days. The diffusion relaxation time for South Bay is similar to that generated by the model, which demonstrates that tidal mixing (diffusion) processes determine the transport there. In North Bay the diffusion time-scale (130 days) is much longer than that determined by the model, so that advective processes dominate there.

Problems which could be addressed by the model but which have not been considered here include the effects of evaporation and precipitation on the salinity variability, the effects of topographic changes for paleoclimate studies of salinity variability and the application of the model to long-term biogeochemical studies.

There are limitations associated with the use of the interpretive long-term model. Fresh water and other materials from point sources are not shared between those water masses which pass the sources during a tidal excursion, but are assumed to disperse (diffuse) as the materials advect with the residual currents. The temporal analogue of this spatial deficiency is the neglect of tidal correlations between variables at a fixed point (Uncles, 1988). In the case of salinity stratification, this is equivalent to ignoring the intratidal, flood–ebb variability in stratification and assuming that an average amount of vertical mixing over a tide, combined with the gravitational circulation and long-term, horizontal salinity gradients, leads to a realistic approximation of the tidally averaged, instantaneous stratification. Further limitations result from the use of lateral averaging, in which it is understood that the model is generating estimates of sectionally averaged quantities in both levels of a segment. The use of a fixed, upper-level thickness also is a limitation in the presence of a halocline, unless the halocline depth and upper-level thickness coincide.

In application to the Bay, the long-term model has been used to aid interpretation of

data, rather than to predict the fate of outfall effluents or other variables of direct water quality management concern. It is considered to be useful in this interpretative respect. Tidal correlations which are ignored in the model can be shown to be small provided intratidal changes in cross-sectional areas (compared with tidally averaged areas) and tidal excursion lengths (compared with estuary lengths) are small (Uncles, 1988). The average RMS water level variation at the Golden Gate is about 0.5 m, which is much smaller than typical Bay depths of around 10 m [Fig. 1(a)]. Relative intratidal changes in cross-sectional areas will be similarly small. Typical RMS current speeds in the Bay are 0.5 m s^{-1} [Cheng *et al.*, 1993] so that the amplitudes of tidal excursions will typically be about 5 km, or ~2 segment lengths. These amplitudes are much less than the lengths of the North and South Bay Branches and are close to the limit of spatial resolution in the model. In view of this, interpretations and conclusions based on general features and trends of the model are considered to be applicable to the real Bay. Quantitative values of modelled salinity, stratification and circulation apply to a 5 m upper-level thickness and tidally averaged behaviour. Application of the model to different types of estuaries, such as those with strong stratification and spatially varying halocline depths, and those with much greater water level variation to depth ratios, is envisaged to be less useful.

6. CONCLUSIONS

Data have been presented on the long-term behaviour of salinity in San Francisco Bay. A width averaged, two-level model of the residual circulation and tidally averaged salinity was developed to interpret long-term (spring–neap and months–years) salinity variability in the Bay. Salient conclusions from the analysis are as follows.

Observed, monthly averaged surface salinity at Stas 1–7 showed pronounced seasonal signals over the 22-yr period, 1967–1988, which were related to the seasonal variability in freshwater inflows. At Stas 3–7 the water was sometimes fresh during periods of strong freshwater inflows. Modelled and observed, monthly averaged surface salinity showed reasonable agreement at Stas 1 and 2, close to the coastal sea, and at Stas 5–7 in the upper reaches of North Bay, close to the Delta. The agreement was less satisfactory in the central reaches of North Bay, where longitudinal salinity gradients were largest at low inflows. Pooling these data, the mean and standard deviation of modelled minus observed salinity data are, respectively, −0.6 (6% of the mean observed salinity at Stas 1–7) and 2.0 (17% of the standard deviation of observed salinity).

Salinity distributions in the upper reaches of North Bay were sensitive to freshwater inflow and this was reflected in a daily variability in both observed and simulated data. Simulated and observed daily data were in good agreement in this region. Simulated values of daily and monthly averaged FSI locations had a pronounced seasonal variability and monthly-averaged locations showed an approximately linear response to the logarithm of monthly averaged Delta inflow.

In South Bay the modelled salinity stratification over the 22-yr period was <8 and the modelled, relatively slow gravitational circulation could change direction with increasing Delta inflow as horizontal salinity gradients reversed in the northern part of South Bay, leading to a salinity maximum there.

In North Bay, modelled stratification at the entrance and midway through San Pablo Bay reached maxima of about 10 with increasing freshwater inflow and subsequently decreased as inflow continued to increase. This decrease in stratification at large inflow

was the result of reduced upper-level and lower-level salinities as the FSI moved down-estuary and came closer to these sites. A similar pattern of modelled stratification and gravitational circulation to that simulated in San Pablo Bay occurred at Stas 3 and 4, although stratification and gravitational circulation at Sta. 4 were much smaller because of shallower depths and lower salinities there. At Stas 5–7, stratification maximized at the lowest freshwater inflows.

Observed salinity from near-surface and near-bed at the San Pablo Bay entrance to Carquinez Strait showed marked tidal variations in stratification. Neap-tide stratification was much stronger than spring-tide stratification. This spring–neap variation in stratification also was simulated by the long-term salinity model. A feature of the modelled data throughout the Bay was the hysteresis in stratification over a spring–neap cycle, in which for a given spring–neap tidal range and fairly steady inflows, the stratification was higher progressing from neaps to springs than from springs to neaps.

Observed data on the vertical structure of longitudinal residual currents from the San Pablo Bay entrance to Carquinez Strait showed a gravitational circulation with pronounced spring–neap modulations. Gravitational circulation increased in strength during neap tides. The simulated, upper-level residual current near this site showed similar spring–neap characteristics. Currents in the upper level achieved their greatest speeds at times of maximum simulated stratification. There was an associated negative correlation between the speed of the simulated gravitational circulation and the spring–neap tidal state. This modelled, spring–neap control on gravitational circulation occurred throughout most of North Bay at moderate freshwater inflows. Observed and modelled gravitational circulations were not always continuous throughout North Bay and in shallow areas could be masked by inflow-induced, down-estuary currents during higher inflows.

An applied, sinusoidal perturbation in coastal salinity with a period of 1 yr propagated and decayed as it moved into the Bay. The signal height reached 50% of its coastal value in Carquinez Strait in the North Bay and near the head of South Bay. The salinity perturbation required about 10 days to propagate from the coastal boundary to the confluence of the South and North Bay Branches. It required about 45 and 40 days to propagate from the coastal boundary to the Delta and to the head of South Bay.

A salinity pulse, applied with a duration of 1 day at the coastal boundary, propagated into the Bay and rapidly decayed, reaching 17% of its coastal boundary value at the confluence of the South and North Bay Branches. The pulse rise times varied from zero at the coastal boundary to about 25–30 days at the heads of the Branches. The pulse's 90% fall times varied from zero at the coastal boundary to about 50 days at the head of North Bay and 65 days at the head of South Bay.

A Delta inflow perturbation with a 1-yr period generated freshwater fraction responses throughout the Bay which were zero in the freshwater inflows of the Delta and of South Bay (because the freshwater fractions there were unity) and which were very small at the coastal boundary. Under low inflow conditions, maximum freshwater fraction responses occurred in the region of highest horizontal salinity gradients between San Pablo and Suisun Bays. The freshwater fraction responses within the Golden Gate and North Bay Branches maximized between 12 and 21 days after the inflow maximum. Lag times were a minimum in the low inflow region of high horizontal salinity gradients. The signal peak required about 50 days to reach the head of South Bay.

A Delta inflow pulse, with a duration of 1 day, generated a freshwater fraction response throughout the Bay with a pulse height which, relative to its Bay averaged value, was very

similar to that exhibited by the 1-yr sinusoidal perturbation. The pulse rise times were <7 days throughout the Golden Gate and North Bay Branches and increased to 35 days at the head of South Bay, consistent with other time-scales there. The 90% fall times varied between 20 and 50 days throughout the Golden Gate and North Bay Branches and increased from 50 to 75 days between the mouth and head of South Bay.

In the Golden Gate and North Bay Branches, these perturbation time-scales were consistent with (1) advection due to lower-level, up-estuary transport of coastal salinity perturbations and (2) both upper-level, down-estuary advection and much faster, down-estuary migration of isohalines (in response to inflow volume continuity) for the inflow perturbation. In South Bay, the dominant time-scales were governed by tidal dispersion.

REFERENCES

Boicourt W. C. (1992) Influences of circulation processes on dissolved oxygen in the Chesapeake Bay. In: *Oxygen Dynamics in the Chesapeake Bay*, D. E. Smith, M. Leffler and G. Mackiernan, editors, Maryland Sea Grant College, University of Maryland, pp. 7–60.

Cayan D. R. and D. H. Peterson (1989) The influence of North Pacific atmosphere circulation in streamflow in the west. *Geophysical Monograph*, **55**, 375–397.

Cayan D. R. and D. H. Peterson (1993) Spring climate and salinity in the San Francisco Bay Estuary. *Water Resources Research*, **29**, 293–303.

Cheng R. T. and J. W. Gartner (1985) Harmonic analysis of tides and tidal currents in South San Francisco Bay, California. *Estuarine, Coastal and Shelf Science*, **21**, 57–74.

Cheng R. T., S. Feng and P. Xi (1989) On inter-tidal transport equation. In: *Estuarine Circulation*, B. J. Neilson, J. Brubaker and A. Kuo, editors, Humana, pp. 133–156.

Cheng R. T., V. Casulli and J. W. Gartner (1993) Tidal, residual, intertidal mudflat (TRIM) model and its applications to San Francisco Bay, California. *Estuarine, Coastal and Shelf Science*, **36**, 235–280.

Cloern J. E. (1984) Temporal dynamics and ecological significance of salinity stratification in an estuary. *Oceanologica Acta*, **7**, 137–141.

Cloern J. E. (1987) Turbidity as a control on phytoplankton biomass and productivity in estuaries. *Continental Shelf Research*, **7**, 1367–1381.

Cloern J. E. (1991a) Annual variation in river flow and primary production in the South San Francisco Bay Estuary. In: *Estuaries and Coasts: Spatial and Temporal Intercomparisons*, M. Elliott and D. Ducrotoy, editors, Olsen and Olsen, Fredensborg, Denmark, pp. 91–96.

Cloern J. E. (1991b) Tidal stirring and phytoplankton bloom dynamics in an estuary. *Journal of Marine Research*, **49**, 203–221.

Conomos T. J. and D. H. Peterson (1977) Suspended-particle transport and circulation in San Francisco Bay: an overview. In: *Estuarine Processes*, Volume 2, Academic Press, New York, pp. 82–97.

Conomos T. J., R. E. Smith and J. W. Gartner (1985) Environmental setting of San Francisco Bay. In: *Temporal Dynamics of an Estuary: San Francisco Bay*, J. E. Cloern and F. H. Nichols, editors, Dr W. Junk Publishers, pp. 1–12.

Feng S., R. T. Cheng and P. Xi (1986a) On tide-induced Lagrangian residual current and residual transport 1. Lagrangian residual current. *Water Resources Research*, **22**, 1623–1634.

Feng S., R. T. Cheng and P. Xi (1986b) On tide-induced Lagrangian residual current and residual transport 2. Residual transport with applications in South San Francisco Bay, California. *Water Resources Research*, **22**, 1635–1646.

Ford M., J. Wang and R. T. Cheng (1990) Predicting the vertical structure of tidal current and salinity in San Francisco Bay, California. *Water Resources Research*, **26**, 1027–1045.

Fischer H. B., E. J. List, R. C. Y. Koh, J. Imberger and N. H. Brooks (1979) *Mixing in Inland and Coastal Waters*, Academic Press, New York, pp. 484.

Hager S. W. and L. E. Schemel (in press) Dissolved inorganic nitrogen, phosphorus, and silicon in South San Francisco Bay. I. Major factors affecting distributions. In: *Climate of San Francisco Bay*, J. T. Hollibaugh, editor, AAAS.

Kimmerer W. and S. Monismith (1993) An estimate of the historical 2 ppt salinity in the San Francisco Bay

Estuary. Appendix A. In: *Managing Freshwater Discharge to the San Francisco Bay/Sacramento–San Joaquin Delta Estuary: The Scientific Basis for an Estuarine Standard*, Report to San Francisco Estuary Project, San Francisco, pp. A1–A29.

Munk W. H. and E. R. Anderson (1948) Note on the theory of the thermocline. *Journal of Marine Research*, **7**, 276–295.

Officer C. B. (1976) *Physical Oceanography of Estuaries (and Associated Coastal Waters)*, Wiley, New York, pp. 465.

Perrels P. A. J. and M. Karelse (1982) A two-dimensional, laterally-averaged model for salt intrusion in estuaries. Technical Report 262, Delft Hydraulics Laboratories, The Netherlands, pp. 483–535.

Peterson D. H., T. J. Conomos, W. W. Broenkow and P. C. Doherty (1975) Location of the non-tidal current null zone in northern San Francisco Bay. *Estuarine and Coastal Marine Science*, **3**, 1–11.

Peterson D. H., J. F. Festa and T. J. Conomos (1978) Numerical simulation of dissolved silica in the San Francisco Bay. *Estuarine and Coastal Marine Science*, **7**, 99–116.

Peterson D. H., D. R. Cayan, J. DiLeo-Stevens and T. G. Ross (1987) Some effects of climate variability in western North America. In: *The Influence of Climate Change and Climatic Variability on the Hydrologic Regime and Water Resources (Proceedings of the Vancouver Symposium, August* 1987), IAHS Publ. No. 168, pp. 45–62.

Peterson D. H., D. R. Cayan, J. F. Festa, F. H. Nichols, R. A. Walters, J. V. Slack, S. E. Hager and L. E. Schemel (1989) Climate variability in an estuary: effects of riverflow on San Francisco Bay. *Geophysical Monograph*, **55**, 419–442.

Proudman J. (1953) *Dynamical Oceanography*, Methuen, London, 409 pp.

San Francisco Estuary Project (1993) *Managing Freshwater Discharge to the San Francisco Bay/Sacramento–San Joaquin Delta Estuary: The Scientific Basis for an Estuarine Standard*. Report to San Francisco Estuary Project, San Francisco, 17 pp + 5 Appendices.

Schemel L. E. and S. W. Hager (in press) Dissolved inorganic nitrogen, phosphorus, and silicon in South San Francisco Bay. II. A case study of effects of local climate and weather. In: *Climate of San Francisco Bay*, J. T Hollibaugh, editor, AAAS.

Smith M. G. (1967) *Theory of Partial Differential Equations*, Van Nostrand, London, 214 pp.

Smith L. H. and R. T. Cheng (1987) Tidal and tidally averaged circulation characteristics of Suisun Bay, California. *Water Resources Research*, **23**, 143–155.

Smith P. E. and R. T. Cheng (1989) Recent progress on hydrodynamical modeling of San Francisco Bay, California. In: *Estuarine and Coastal Modeling Conference Proceedings*, WW Division of the American Society of Civil Engineers, Newport, RI, pp. 502–510.

Smith P. E., R. T. Cheng, J. R. Burau and M. R. Simpson (1991) Gravitational circulation in a tidal strait. In: *Hydraulic Engineering* 1991 *Conference Proceedings*, WW Division of the American Society of Civil Engineers, Nashville, TN, pp. 429–434.

Uncles R. J. (1988) Coupling of hydrodynamic and ecosystem modelling applied to tidal estuaries. In: *Coastal-Offshore Ecosystem Interactions. Lecture Notes on Coastal and Estuarine Studies*, B.-O. Jansson, editor, Springer-Verlag, pp. 309–356.

Uncles R. J. and D. H. Peterson (1995) A computer model of long-term salinity in San Francisco Bay: sensitivity to mixing and inflows. *Environment International*, **21**, 647–656.

Walters R. A. and J. W. Gartner (1985) Subtidal sea level and current variations in the northern reach of San Francisco Bay. *Estuarine, Coastal and Shelf Science*, **21**, 17–32.

Walters R. A., R. T. Cheng and T. J. Conomos (1985) Time scales of circulation and mixing processes of San Francisco Bay waters. In: *Temporal Dynamics of an Estuary: San Francisco Bay*, J. E. Cloern and F. H. Nichols, editors, Dr W Junk Publishers, pp. 13–36.